IEEE Access
Multidisciplinary | Rapid Review | Open Access Journal

Received December 29, 2020, accepted January 15, 2021, date of publication January 22, 2021, date of current version February 5, 2021.

Digital Object Identifier 10.1109/ACCESS.2021.3053773

Large Intelligent Surfaces With Discrete Set of Phase-Shifts Communicating Through Double-Rayleigh Fading Channels

FELIPE A. P. DE FIGUEIREDO[1,2], MICHELLE S. P. FACINA[1], RICARDO COELHO FERREIRA[1], YUN AI[3], (Member, IEEE), RUKHSANA RUBY[4], QUOC-VIET PHAM[5], (Member, IEEE), AND GUSTAVO FRAIDENRAICH[1]

[1]DECOM/FEEC, State University of Campinas (UNICAMP), Campinas 13083-852, Brazil
[2]Instituto Nacional de Telecomunicações (INATEL), Santa Rita do Sapucaí 37540-000, Brazil
[3]Faculty of Engineering, Norwegian University of Science and Technology, 2815 Gjøvik, Norway
[4]College of Computer Science and Software Engineering, Shenzhen University, Shenzhen 518060, China
[5]Research Institute of Computer, Information and Communication, Pusan National University, Busan 43241, South Korea

Corresponding author: Felipe A. P. de Figueiredo (felipe.figueiredo@inatel.br)

This work was supported in part by the European Union's Horizon 2020 Research and Innovation Program through the ORCA Project under Grant 732174, in part by the São Paulo Research Foundation (FAPESP) under Grant 2016/16181-2, in part by the Research and Development ANEEL, PROJECT COPEL, and Empresa Brasileira de Pesquisa e Inovação Industrial (EMBRAPII) under Grant 2866-0366/2013, and in part by the CNPq under Grant 304946/2016-8 and Grant 313239/2017-7.

ABSTRACT Despite many studies already published on large intelligent surfaces (LIS), there are still some gaps in mathematical models in the face of possible scenarios. In this work, we evaluate the performance of a single-input single-output (SISO) system in which an LIS acts as a controllable scatterer. We consider that the direct link between the transmitting and receiving devices is non-existent due to a blockage. Quantization phase errors at the LIS are considered since a high precision configuration of the reflection phases is not always feasible. We derive exact closed-form expressions for the spectral efficiencies, outage probabilities, and average symbol error rate (SER) of different modulations schemes. We assume a more comprehensive scenario in which b bits are dedicated to the phase adjustment of the LIS' elements. Based on Monte Carlo simulations, we prove the excellent accuracy of our approach and investigate the behavior of the power scaling law and the power required to reach a specific capacity, depending on the number of reflecting elements. We show that an LIS with approximately fifty elements and four dedicated bits for phase quantization outperforms the conventional system without LIS.

INDEX TERMS Large intelligent surface, outage probability, quantization phase errors, spectral efficiency, symbol error rate.

I. INTRODUCTION

There is no doubt that quantization errors are inevitable when using analog-to-digital converters (ADCs). These converters bridge the analog and the digital worlds, and the lower is their resolution, the more distortions they can cause to the conversion process. Since the rounding quantization introduces error in the signal estimation stage, Hou *et al.* [1] propose a quantization error reduction scheme for detection based on orthogonal lattices. On the other hand, Kotera *et al.* [2] proves that an efficient nonlinear Viterbi-like algorithm, used as the equalization scheme, can estimate both inter-symbol interference in multi-path channel and quantization error in ADC and improve the bit error rate (BER) performance.

For large intelligent surfaces (LIS) assisted systems, little is known about the impact of quantization errors. Also known as reconfigurable intelligent surfaces (RIS), this technology is a strong candidate to be integrated into the sixth generation (6G) of cellular networks. It comes with the promise to satisfy the requirements of reliability, low latency, and high data rates for heterogeneous devices, which the fifth generation (5G) was not able to fully meet [3]. Its structure consists of many electromagnetic elements acting individually as scatterers, capable of jointly reflecting the incident signal to the desired direction [4], [5]. Among its advantages, we can mention the ideally passive nature that does not require any dedicated

The associate editor coordinating the review of this manuscript and approving it for publication was Mohammad S. Khan.

energy source. By not amplifying the incident signal, an LIS provides an inherently full-duplex transmission scheme without introducing noise, unlike relays. It can also be easily installed onto facades of buildings or walls of rooms thanks to its lightweight and conformal geometry. Two strategies are possible due to the smart adjustment of the phase shifts; the reflected signals can add coherently or destructively at the receiver. The first strategy improves the received signal power, while the second one avoids interference of unwanted signals or transmitters and increases the security of the communication system [6].

There are several questions still open regarding LIS-assisted communications systems. One of them is which frequency band is more suitable for its deployments? In fact, there are theoretical and proofs-of-concept works for all of these frequency bands [7]–[19]. In [20], Emil Björnson points out that it might still be too early to say in which frequency band LIS will be most useful, despite listing some points that deserve our attention. At lower frequencies, existing relaying technology is rather competitive, and the propagation conditions are quite good. However, LIS-assisted systems present some potential advantages over traditional relaying techniques such as full-duplex communications, reduced power consumption, and hardware cost for low and high-frequency bands (since there is no need for power amplifiers) [7], [9], [11]–[13], [19]. According to several works [20]–[25], LIS technology can do something new for mmWave frequencies and above such as (i) adding extra propagation paths to sparse channels, (ii) replacing the need for large antenna arrays since they are complicated to build and (iii) working as relay since conventional relays might not be available.

Most studies have focused on optimizing the reflection coefficients (*i.e.*, amplitude and phase) of each LIS element. For example, Zhang *et al.* believes that LIS can play critical roles in beyond 5G networks [26]. Assuming deterministic flat-fading channels and, so with a low-rank multiple-output multiple-input (MIMO) channel, the authors show that simply deploying multiple optimal LIS elements can guarantee performance gains due to spatial multiplexing. Still considering multiple users, Han *et al.* elaborate on two algorithms to jointly optimize the transmit beamforming at the BS and the phase shifts at the LIS under the quality of service (QoS) constraints [27]. From derived lower bounds of the transmit power concerning the number of BS antennas, the number of LIS elements, and the number of mobile users, they show that the transmit power at the BS is significantly lower than that of a communications system without LIS.

However, it is worth mentioning that the reflection phases' high precision configuration is unfeasible. In practice, the number of bits is limited, and as a consequence, the phase quantization errors arise. Before proposing techniques to reduce them, we first need to know them and estimate their effects as closely as possible to reality.

In this work, we deviate a little from this idea and look for more precise mathematical models under more practical scenarios. In our previous work [28], we employed the central limit theorem (CLT) to derive the bit error rate when there are phase estimation errors. However, it is known that the CLT is inaccurate when the number of elements in LIS is small, and the approximation error can be significant in the high signal-to-noise ratio (SNR) regime.

Following the same reasoning, Badiu and Coon [29] do a preliminary analysis based on a limited number of imperfect reflectors. They conclude that the LIS- assisted SISO system is equivalent to a point-to-point communication over a Nakagami fading channel, and the performance measured from the error probability is robust against the phase errors. Abeywickrama *et al.* [30] was the pioneering work to consider a practical phase-shift model in which the amplitude is dependent on the phase in the re?ection coefficient. From [30], simulation results unveil a substantial performance gain achieved by the joint beamforming optimization when compared to the conventional ideal model. On the other hand, Han *et al.* [31] propose an optimal phase shift design that achieves approximately the ergodic capacity and demonstrates that a quantizer with two bits is sufficient for a capacity degradation below 1 bit/s/Hz. The multi-user multi-input single-output downlink LIS-assisted system harvests power from the received signals in [32]. Hu *et al.* show that small bit-resolution discrete phase shifters are sufficient to tightly approximate the sum-rate of an ideal case with continuous phase shifters. In [33], Wang *et al.* consider a SISO LIS-assisted system and derive exact expressions for outage probability and diversity order without employing a CLT approach. However, they assume that each element of the LIS has only a one-bit phase shifter. Based on this one-bit assumption, they derive the outage probability, which only works in high SNR regimes.

From the works mentioned above, we can see that LIS-assisted wireless systems' performance has mainly been assessed in terms of symbol error rate (SER) lower-bounds, with perfect or very limited phase generation (*e.g.*, one-bit resolution shifters), besides employing CLT to approximate SNR distributions. In this article, we present an in-depth investigation of SISO systems in the presence of quantization errors, which are introduced by the LIS' reflecting elements. Our focus is to demonstrate a theoretical framework that quantifies the performance based on an accurate approximation of the SNR distribution when the LIS's reflecting elements can only generate phases out of a discrete set. Additionally, an analytic comparison between LIS-assisted and non-assisted systems in terms of spectral efficiency, average SNR, and required transmit power is carried out. Therefore, this paper's contribution can be summarized as follows.

- Novel and exact analytical expressions for the probability density function (PDF) and cumulative density function (CDF) of the instantaneous SNR are derived, considering the number of reflecting elements, a discrete set of possible phases, and assuming that the Source-RIS and RIS-Destination links experience Rayleigh fading.
- Considering the composite channel between source and destination as the double (cascaded) Rayleigh fading

channel [34]–[37], we derive the average SNR for the LIS-assisted wireless system.
- In order to study the outage performance, we derive a closed-form expression for the outage probability, which provides useful insights and can be employed as a design tool.
- We provide a closed-form expression for the average SER of some modulation schemes for the LIS-assisted system. Additionally, a tight approximation for the average SER in the high-SNR regime is derived.
- Based on high-SNR SER approximation, we derive a closed-form expression for the diversity order of the LIS-assisted system, which shows that the diversity order increases with the number of reflecting elements.
- Exact analytical expressions for the ergodic spectral efficiency of the LIS-assisted system are also found. Additionally, tight high-SNR and lower/upper bounds approximations are derived for the spectral efficiency.
- We present an analysis of the power scaling law and the power required to achieve specific capacities. These results show that the transmit power can be reduced proportionally to $1/N^2$ without compromising the spectral efficiency. This power reduction is paramount to power-constrained devices such as the internet of things (IoT) ones.
- Based on the tight approximation of the instantaneous SNR' PDF, we can evaluate the system performance as the number of bits and reflectors increases. We conclude that a LIS with approximately fifty elements and four bits dedicated to phase quantization outperforms a conventional SISO system's performance without a LIS. To the best of our knowledge, no similar results have been found in the literature.

Several works in the literature [27], [31], [38]–[42] consider cases where it is possible to position a LIS so that there is a line-of-sight (LoS) link, at least, between the BS and the LIS itself. However, we envision indoor environments where there might not be LoS links at all. Therefore, we analyze and compare the performance of an LIS-assisted system to a conventional SISO one with no LoS link. Our results demonstrate that a LIS equipped with enough reflecting elements can improve a wireless system's performance even though there are no LoS links between any of the involved entities (*i.e.*, Source, Destination, and LIS).

The remainder of this article is organized as follows: Section II presents the adopted model and the preliminary assumptions. In Section III, we derive exact closed-form expressions for some important performance metrics and evaluate the quantization error effects. Section IV shows our setup and the results obtained from simulations with that. Finally, Section V summarizes the main conclusions.

Notations: Scalars are denoted by italic letters while vectors and matrices, by bold-face lower-case and upper-case letters, respectively. For a complex-valued vector x, $|x|$ denotes its Euclidean norm and diag(x) represents the diagonal matrix. The distribution of a circularly symmetric complex Gaussian (CSCG) random vector with mean fx and covariance Ξ is denoted by $\mathcal{CN}(x, \Xi)$; and $\sim$ stands for "distributed as". For any general vector x, x_i denote its ith element while $\mathbb{E}$ is the statistical expectation. Finally, Pr(.) represents the probability of a specific event occurring.

II. SYSTEM MODEL

The system model of the adopted LIS-assisted communications scheme is typical of indoor environments and can be seen in Figure 1. Here, the fading channels g_n and h_n between the single-antenna source (S) and the n-th antenna (or reflecting) element of the LIS, and the nth antenna element of the LIS and the single-antenna destination (D), respectively, are assumed to be independent, identical, slowly varying, flat, and their envelopes follow Rayleigh distributions, *i.e.*, $g_n \sim \mathcal{CN}(0, \beta_g)$ and $h_n \sim \mathcal{CN}(0, \beta_h)$. This assumption, used in several previous works including [43]–[47] and references therein, originates from the fact that even if the LoS links between S and D, between S and the LIS, and between the LIS and D are blocked, there still exist extensive number of scatters. Also, the direct signal path between S and D is neglected due to unfavorable propagation conditions that might be caused by an obstacle, for example.

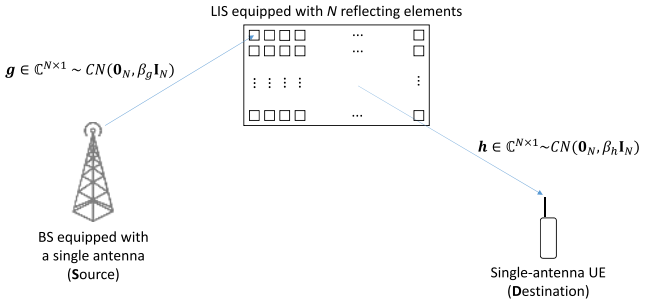

FIGURE 1. System model of the LIS-assisted wireless system.

The parameters β_g and β_h model the shadow and geometric attenuation fading (*i.e.*, the large-scale fading coefficients), which are assumed to be independent over the elements of LIS and change very slowly over time. They are constant over several coherence-time intervals [48], since the distance between devices and LIS is much larger than the distance between the LIS' elements. In this far-field regime [4], the intelligent surface is better modeled as a scatterer and the scaling law that governs the intensity of its electric field is a function of the distances' product, as proved in [49] and shown later.

We assume that the LIS is a reflect-array composed of N simple and re-configurable reflector elements connected to a controller. Additionally, we assume that the phase-shifts produced by the channels are estimated perfectly [15]. However, the desired phases cannot be accurately generated by the LIS once it has a discrete set of phases. Practical LISs have a limited number of phase shifts, *i.e.*, a discrete set of phase-shifts constrained by the number of quantization bits (also known as phase resolution) of the LIS. The number of

quantization bits is denoted by b. Therefore, the set of phase shifts produced by each one of the elements of the LIS is defined as

$$\phi_n = \left\{0, \frac{2\pi}{2^b}, \frac{4\pi}{2^b}, \cdots, \frac{2\pi(2^b-1)}{2^b}\right\}. \quad (1)$$

Therefore, we model the deviation from the correct/ideal phase-shift as a phase-noise, δ_n, which is uniformly distributed in the range $[-\pi/Q, \pi/Q]$, where $Q = 2^b$ is the number of discrete phases the LIS can generate [50] dictated by the hardware complexity and power consumption of LIS.

III. INTELLIGENT TRANSMISSION THROUGH LIS

In slowly varying flat fading channels, the signal received at the destination after being reflected through an LIS composed of N passive elements can be written as

$$y = \sqrt{\rho}\left[\sum_{n=1}^{N} g_n e^{-j\phi_n} h_n\right] s + w, \quad (2)$$

where ρ is the average SNR, ϕ_n is the adjustable phase-shift produced by the nth LIS reflector, s is the modulation data symbol with zero mean, $\mathbb{E}[|s|^2] = 1$, and $w \sim \mathcal{CN}(0, 1)$ is the additive white Gaussian noise (AWGN) term. Then, (2) can be re-written in the matrix-form as

$$y = \sqrt{\rho} h^T \Phi g s + w, \quad (3)$$

where $g = [g_1, \cdots, g_N]^T$ and $h = [h_1, \cdots, h_N]^T$ are the channel coefficient vectors between the BS and the RIS and between the RIS and the terminal, respectively, while $\Phi = \text{diag}\left(\left[e^{-j\phi_1}, \cdots, e^{-j\phi_N}\right]\right)$ is the diagonal matrix containing the phase-shifts applied by the elements of the LIS.

It can be noticed that (3) is similar to the equation of conventional MIMO systems employing precoding/beamforming for transmission. However, differently from those systems, where precoding/beamforming is carried out at the transmitter side, here it is carried out over the transmission medium (*i.e.*, the environment) [15].

The complex channels can be written in polar representation (*i.e.*, with magnitude and phase) as $h_n = \alpha_n e^{j\theta_n}$ and $g_n = \xi_n e^{j\psi_n}$, therefore, (2) can be re-written as

$$\begin{aligned} y &= \sqrt{\rho}\left[\sum_{n=1}^{N} \alpha_n \xi_n e^{j(\theta_n+\psi_n-\phi_n)}\right] s + w \\ &= \sqrt{\rho}\left[\sum_{n=1}^{N} \alpha_n \xi_n e^{j\delta_n}\right] s + w, \end{aligned} \quad (4)$$

where the second line is obtained from the assumption that the LIS only generates discrete phases and consequently, there is a phase-noise, $\delta_n = \theta_n + \psi_n - \phi_n$. The term inside the square brackets represents the composite channel coefficient and gives clues that the system diversity gain depends on the number of LIS' reflecting elements, N.

Considering the phase-noise, then the instantaneous SNR at the destination is given by

$$\gamma = \rho\left|\sum_{n=1}^{N} \alpha_n \xi_n e^{j\delta_n}\right|^2. \quad (5)$$

Note that the instantaneous SNR is maximized when $\delta_n = 0$, *i.e.*, the channels are correctly estimated, and the LIS can accurately generate the phases induced by the channels (meaning that $Q \to \infty$) [51].

Lemma 1: From empirical comparisons between the normalised histogram of the random variable given by

$$r = \sqrt{\rho}\left|\sum_{n=1}^{N} \alpha_n \xi_n e^{j\delta_n}\right| = \sqrt{\rho}\left|\sum_{n=1}^{N} |g_n||h_n| e^{j\delta_n}\right|, \quad (6)$$

and the theoretical PDF of a Gamma random variable, it is possible to say that the PDF of r can be accurately approximated by the Gamma PDF with shape and scale parameters given by κ and θ, respectively as

$$\kappa = \frac{-\left(\mathbb{E}[\gamma^2] - 5\mathbb{E}[\gamma]^2\right) + \sqrt{\mathbb{E}[\gamma^2]^2 - 34\mathbb{E}[\gamma^2]\mathbb{E}[\gamma]^2 + 49\mathbb{E}[\gamma]^4}}{2\left(\mathbb{E}[\gamma^2] - \mathbb{E}[\gamma]^2\right)} > 0, \quad (7)$$

$$\theta = \sqrt{\frac{-\sqrt{\mathbb{E}[\gamma^2]^2 + 14\mathbb{E}[\gamma^2]\mathbb{E}[\gamma]^2 + \mathbb{E}[\gamma]^4} + 2\mathbb{E}[\gamma^2] + 2\mathbb{E}[\gamma]^2}{6\mathbb{E}[\gamma]}} > 0, \quad (8)$$

where $\mathbb{E}[\gamma]$ and $\mathbb{E}[\gamma^2]$ are given by (9) *and* (10)*, as shown at the bottom of the next page, respectively.*

Some examples of this comparison are shown in Section IV. The parameters κ and θ are found following the rationale presented in Appendix A. Therefore, the PDF of γ can be found following the standard transformation of random variables, $\gamma = r^2$, and is defined as

$$f_\gamma(\gamma) = \frac{1}{2\Gamma(\kappa)\theta^\kappa} \gamma^{\left(\frac{\kappa-2}{2}\right)} e^{-\frac{\sqrt{\gamma}}{\theta}}, \gamma \geq 0. \quad (11)$$

In its turn, the CDF of the SNR random variable, γ, is defined as

$$F_\gamma(\gamma) = \int_0^\gamma f_\gamma(x)dx = 1 - \frac{\Gamma\left(\kappa, \frac{\sqrt{\gamma}}{\theta}\right)}{\Gamma(\kappa)}, \gamma \geq 0, \quad (12)$$

where $\Gamma(.)$ is the Euler gamma function while $\Gamma(.,.)$ is the upper incomplete gamma function. The integral result is obtained by directly applying (Eq. 2.33.10, [52]).

From (9), it is clear that the diversity gain of the LIS-assisted system can be calculated as

$$G_{\text{LIS}} = \beta_g \beta_h \mathcal{A}_1, \quad (13)$$

which can be improved by increasing the number of LIS' reflecting elements, N, and/or the number of quantization levels, Q.

Remark 1: When $Q \to \infty$, i.e., the LIS is able to generate any phase-shift, the phase-noise is zero, $\delta_n = 0, \forall n$, and consequently, (9) and (10) can be simplified to (14) and (15), as shown at the bottom of the next page, respectively, and whose derivations are presented in Appendix B.

A. EXACT ERGODIC SPECTRAL EFFICIENCY

The ergodic spectral efficiency of the LIS-assisted system is defined as

$$C = \mathbb{E}\left[\log_2(1+\gamma)\right] = \int_0^\infty \log_2(1+\gamma) f_\gamma(\gamma) d\gamma, \tag{16}$$

whose exact closed-form expression obtained through an integral solver [53] is given by (17), as shown at the bottom of the next page. Here, ${}_pF_q\left(a_1, \cdots, a_p; b_1, \cdots, b_q; z\right)$ is the generalized hypergeometric function [54] and $\Psi^{(n)}(z)$ is the nth derivative of the digamma function, also known as the polygamma function [55].

Remark 2: In high SNR regime, the ergodic spectral efficiency in (17) can be approximated as in (18), as shown at the bottom of the next page.

Remark 3: When $\rho \to \infty$, then (17) becomes

$$\lim_{\rho\to\infty} C = \frac{4\log(\theta)}{\log(4)}. \tag{19}$$

Remark 4: In high SNR and large N regimes, the ergodic spectral efficiency can be approximated as

$$C_{\text{high-SNR, }N} \approx \frac{2}{\theta^2(\kappa-1)(\kappa-2)\log(4)} + \frac{4(\log(\theta)+\psi^{(0)}(\kappa))}{\log(4)}. \tag{20}$$

The proofs for Remarks 2, 3 and 4 are presented in Appendices C, D and E, respectively.

Remark 5: For large N, the ergodic spectral efficiency can be approximated as

$$C_N \approx \frac{2}{\log(4)}\left[\frac{1}{\theta^2(\kappa-1)(\kappa-2)} + 2\psi^{(0)}(\kappa)\right]. \tag{21}$$

This remark is obtained after comparing (19) and (20). This way, we obtain the improvement achieved by increasing the value of N because (19) corresponds to the case where the SNR goes to infinity and (20) corresponds to the case when both SNR and N go to infinity.

Other alternative to find the expectation in (16) is using the PDF of the random variable given by $C_{\text{inst.}} = \log_2(1+\gamma)$, *i.e.*, the instantaneous spectral efficiency, which can be found after applying standard transformation of random variables to (11) giving rise to

$$f_{C_{\text{inst.}}}(c) = \frac{\log(2)}{\Gamma(\kappa)\theta^\kappa} 2^{c-1}(2^c-1)^{\left(\frac{\kappa-2}{2}\right)} e^{-\frac{\sqrt{2^c-1}}{\theta}}, \; c \geq 0. \tag{22}$$

Then, the CDF of the instantaneous spectral capacity random variable is expressed by

$$F_{C_{\text{inst.}}}(c) = \int_0^c f_{C_{\text{inst.}}}(x)\, dx = 1 - \frac{\Gamma\left(\kappa, \frac{\sqrt{2^c-1}}{\theta}\right)}{\Gamma(\kappa)}, \tag{23}$$

whose integral is also found by directly applying (Eq. 2.33.10, [52]).

B. UPPER AND LOWER-BOUNDS FOR THE ERGODIC SPECTRAL EFFICIENCY

As it can be seen, (17) is quite complex. Therefore, here we aim at finding simpler but yet tight bounds for the ergodic spectral efficiency of the LIS-assisted system. According to Jensen's inequality [48], it holds that

$$\mathbb{E}\left[\log_2(1+\gamma)\right] \leq \log_2(1+\mathbb{E}[\gamma]). \tag{24}$$

Then, by using $\mathbb{E}[\gamma]$, which is given by (9), a possible upper-bound for the ergodic capacity of the LIS-assisted system can be given by (25), as shown at the bottom of the next page. As it is tight for high SNR scenarios, it can be assumed as a good approximation. Additionally, it is seen that the ergodic spectral efficiency is an increasing function of ρ, N and Q. By looking at (25), we see that Q can be canceled out due to the fact that $\sin(\pi/Q) \approx \pi/Q$ when Q is large enough (*e.g.*, $Q \geq 16$). Therefore, when Q is sufficiently large, further increasing the number of quantization levels, Q, does not have any noticeable impact on the systems' performance. This is also evidenced by the results shown in Figures 5 and 6. Instead, when Q is large enough, the upper-performance limit improvement poses a better than the linear relationship with N, which is better seen in (28), as shown at the bottom of page 7.

On the other hand, again according to Jensen's inequality [48], it holds that

$$\mathbb{E}\left[\log_2(1+\gamma)\right] \geq \log_2\left(1+\left[\mathbb{E}\left[\frac{1}{\gamma}\right]\right]^{-1}\right). \tag{26}$$

$$\mathbb{E}[\gamma] = \mathbb{E}\left[r^2\right] = \rho\beta_g\beta_h\mathcal{A}_1 = \rho\beta_g\beta_h N\left[1+\frac{1}{16}(N-1)Q^2\sin^2\left(\frac{\pi}{Q}\right)\right]. \tag{9}$$

$$\mathbb{E}\left[\gamma^2\right] = \mathbb{E}\left[r^4\right] = \left(\rho\beta_g\beta_h\right)^2\mathcal{A}_2 = \left(\rho\beta_g\beta_h\right)^2\frac{N}{256}\left\{512(N+1) + \frac{32(N-1)Q^2}{\pi^2} + \frac{(N-1)Q^2\left[\pi\sin^2\left(\frac{\pi}{Q}\right)\left((N-2)Q\left(\pi(N-3)Q\sin^2\left(\frac{\pi}{Q}\right)+16\sin\left(\frac{2\pi}{Q}\right)\right)+16\pi(4N+1)\right)-32\cos\left(\frac{4\pi}{Q}\right)\right]}{\pi^2}\right\}. \tag{10}$$

Consequently, by using a tight approximation of $\mathbb{E}[1/\gamma]$ (see Appendix F), a lower-bound for the ergodic capacity of the LIS-assisted system can be derived and given as (27), as shown at the bottom of the page.

Like the SNR, the spectral efficiency is also maximized when $Q \to \infty$, meaning that the LIS has infinite phase-shift precision and can generate any phase-shift. In this case, the maximum ergodic spectral efficiency with the upper and lower bounds are given by (28) and (29), as shown at the bottom of the next page, respectively.

C. IMPACT OF BIT QUANTIZATION IN THE SPECTRAL EFFICIENCY

In practical communication systems, the set of phase-shifts is limited by the number of quantization bits of the LIS, influencing the achieved spectral efficiency directly. Therefore, in this section, we propose a criterion for selecting the number of quantization levels $Q = 2^b$ so that the ergodic spectral efficiency is optimized up to a specific spectral degradation in bits/s/Hz. In order to quantify this degradation, we define the error ϵ brought about by a limited number of phase-shifts as

$$C_{\text{upper}}^{\text{max.}} - C_{\text{upper}} \leq \epsilon. \tag{30}$$

Remark 6: From (30)*, we see that when the number of LIS elements tends to* ∞*, then the ergodic spectral efficiency degradation,* ϵ*, becomes*

$$\lim_{N\to\infty} \epsilon = \log_2\left(\frac{\pi^2}{Q^2 \sin^2(\pi/Q)}\right) \text{ bits/s/Hz}. \tag{31}$$

Remark 7: From (30)*, we see that when* $\rho \to \infty$*, then the ergodic spectral efficiency degradation,* ϵ*, is given by*

$$\lim_{\rho\to\infty} \epsilon = \log_2\left(\frac{16 + (N-1)\pi^2}{16 + (N-1)Q^2 \sin^2(\pi/Q)}\right) \text{ bits/s/Hz}. \tag{32}$$

Proposition 1: In order to guarantee an suitable ergodic spectral efficiency degradation of ϵ *bits/s/Hz compared to an LIS with full-resolution phase-shift, the number of quantization levels, Q, of the LIS should satisfy*

$$Q \sin(\pi/Q) \geq \sqrt{\frac{16\left(2^{-\epsilon}-1\right)}{N\rho\beta_g\beta_h(N-1)} + \frac{16\left(2^{-\epsilon}-1\right)}{N-1} + \pi^2 2^{-\epsilon}}. \tag{33}$$

Remark 8: From (33)*, we see that when* $N \to \infty$*, the number of quantization levels, Q, should satisfy*

$$\lim_{N\to\infty} Q \sin(\pi/Q) \geq \sqrt{2^{-\epsilon}}\pi. \tag{34}$$

$$\lim_{Q\to\infty} \mathbb{E}[\gamma] = \rho\beta_g\beta_h N\left[1 + \frac{(N-1)\pi^2}{16}\right]. \tag{14}$$

$$\lim_{Q\to\infty} \mathbb{E}\left[\gamma^2\right] = \left(\rho\beta_g\beta_h\right)^2 \frac{N}{256}\left[256 + 768N + \pi^4(N-3)(N-2)(N-1) + 48\pi^2(2N-1)(N-1)\right]. \tag{15}$$

$$\begin{aligned} C = {} & \frac{2\,{}_2F_3\left(1, 1; 2, \frac{3}{2} - \frac{\kappa}{2}, 2 - \frac{\kappa}{2}; -\frac{1}{4\theta^2}\right)}{\theta^2(\kappa-1)(\kappa-2)\log(4)} - \frac{2\pi \sec\left(\frac{\pi\kappa}{2}\right)\,{}_1F_2\left(\frac{\kappa}{2} + \frac{1}{2}; \frac{3}{2}, \frac{\kappa}{2} + \frac{3}{2}; -\frac{1}{4\theta^2}\right)}{(\kappa+1)\theta^{\kappa+1}\Gamma(\kappa)\log(4)} \\ & + \frac{2\pi \csc\left(\frac{\pi\kappa}{2}\right)\,{}_1F_2\left(\frac{\kappa}{2}; \frac{1}{2}, \frac{\kappa}{2} + 1; -\frac{1}{4\theta^2}\right)}{\kappa\theta^{\kappa}\Gamma(\kappa)\log(4)} + \frac{4(\log(\theta) + \psi^{(0)}(\kappa))}{\log(4)}. \end{aligned} \tag{17}$$

$$C_{\text{high-SNR}} \approx \frac{2}{\theta^2(\kappa-1)(\kappa-2)\log(4)} - \frac{2\pi \sec\left(\frac{\pi\kappa}{2}\right)}{(\kappa+1)\theta^{\kappa+1}\Gamma(\kappa)\log(4)} + \frac{2\pi \csc\left(\frac{\pi\kappa}{2}\right)}{\kappa\theta^{\kappa}\Gamma(\kappa)\log(4)} + \frac{4(\log(\theta) + \psi^{(0)}(\kappa))}{\log(4)}. \tag{18}$$

$$C \leq C_{\text{upper}} = \log_2\left(1 + N\rho\beta_g\beta_h\left[1 + \frac{1}{16}(N-1)Q^2 \sin^2\left(\frac{\pi}{Q}\right)\right]\right). \tag{25}$$

$$\begin{aligned} C &\geq C_{\text{lower}} \\ &\approx \log_2\left(1 + \frac{\mathbb{E}[\gamma]^3}{\mathbb{E}\left[\gamma^2\right]}\right) \\ &= \log_2\left(1 + \frac{256N^2\rho\beta_g\beta_h\left(\frac{1}{16}(N-1)Q^2 \sin^2\left(\frac{\pi}{Q}\right) + 1\right)^3}{\frac{32(N-1)Q^2}{\pi^2} + \frac{(N-1)Q^2\left(\pi \sin^2\left(\frac{\pi}{Q}\right)\left((N-2)Q\left(\pi(N-3)Q \sin^2\left(\frac{\pi}{Q}\right) + 16 \sin\left(\frac{2\pi}{Q}\right)\right) + 16\pi(4N+1)\right) - 32\cos\left(\frac{4\pi}{Q}\right)\right)}{\pi^2} + 512(N+1)}\right). \end{aligned} \tag{27}$$

Remark 9: From (33) we see that when $\epsilon \to \infty$, then the number of quantization levels, Q, should satisfy

$$\lim_{\epsilon \to \infty} Q \sin(\pi/Q) \leq \pi. \tag{35}$$

After analyzing Remark 9, we notice that the first term in (35) is equal to π only when $Q \to \infty$. Therefore, in order to have no degradation at all, an infinite number of quantization levels is necessary, which demonstrates the correctness of Remark 9.

Summing up, these results can be used to select the precision necessary for an LIS-assisted system to achieve a pre-defined and acceptable degradation in its ergodic spectral efficiency.

D. OUTAGE PROBABILITY

Based on the knowledge of the approximate PDF of the instantaneous spectral efficiency given by (22), it is possible to find its CDF and derive analytical expressions for the outage probability. The outage probability is defined as the probability that the achieved instantaneous spectral efficiency falls below a given threshold $C_{\text{out.}}$ and can be written as

$$\begin{aligned} P_{\text{out.}} &= \Pr\{C_{\text{inst.}} < C_{\text{out.}}\} \\ &= \int_0^{C_{\text{out.}}} f_{C_{\text{inst.}}}(x)\, dx \\ &= 1 - \frac{\Gamma\left(\kappa, \frac{\sqrt{2^{C_{\text{out.}}}-1}}{\theta}\right)}{\Gamma(\kappa)}, \end{aligned} \tag{36}$$

whose proof is provided in Appendix G. From (36), it is possible to observe that, for a fixed outage capacity, $C_{\text{out.}}$ the outage probability, $P_{\text{out.}}$, decreases as N and/or Q increases, *i.e.*, the outage performance improves by adding more reflecting elements and/or increasing the number of quantization bits to the LIS. Conversely, for a constant N, the outage performance decreases as $C_{\text{out.}}$ increases.

Besides that way, the outage probability can also be defined with regard to the instantaneous SNR. In this case,it is the probability that the instantaneous SNR falls below a given SNR threshold $\gamma_{\text{out.}}$. So, the outage probability is given by

$$\begin{aligned} P_{\text{out.}} &= \Pr\{\gamma < \gamma_{\text{out.}}\} \\ &= \int_0^{\gamma_{\text{out.}}} f_{\gamma}(x)\, dx \\ &= \frac{1}{\theta^{\kappa/2}} \left[1 - \frac{\Gamma\left(\kappa, \frac{\sqrt{\gamma_{\text{out.}}}}{\theta}\right)}{\Gamma(\kappa)}\right], \end{aligned} \tag{37}$$

and found by using (94) in Appendix G. It can also be expressed as

$$P_{\text{out.}} = \frac{\gamma^{\frac{\kappa}{2}}}{\kappa \theta^{\frac{3\kappa}{2}}} {}_1F_1\left(\kappa, \kappa+1, -\frac{\sqrt{\gamma}}{\theta}\right). \tag{38}$$

Remark 10: In high SNR regime, the outage probability can be approximated as

$$P_{out.}^{high\text{-}SNR} = \frac{\gamma^{\frac{\kappa}{2}}}{\kappa \theta^{\frac{3\kappa}{2}}}. \tag{39}$$

The proofs of (38) and (39) are provided in Appendix H.

E. AVERAGE SYMBOL ERROR RATE

According to [56], the average SER is defined as the expectation of conditional error probability, $P_{e|\gamma}$, given the distribution of the SNR, γ. For a wide variety of modulation schemes, $P_{e|\gamma}$ is defined as $P_{e|\gamma} = a\mathcal{Q}\left(\sqrt{b\gamma}\right)$, where a and b are constant modulation dependent parameters and $\mathcal{Q}$ is the Gaussian $\mathcal{Q}$-function defined as $\int_x^{\infty} e^{-t^2/2}/\sqrt{2\pi}\, dt$ [56]. Therefore, the average SER is derived as

$$\mathbb{E}\left[a\mathcal{Q}\left(\sqrt{b\gamma}\right)\right] = a\int_0^{\infty} \mathcal{Q}\left(\sqrt{b\gamma}\right) f_{\gamma}(\gamma) d\gamma, \tag{40}$$

and can be analytically expressed by (41), as shown at the bottom of the next page, whose proof is provided in Appendix I. Note that, a and b are constants that depend on the modulation scheme. For instance, the average SER of the binary phase shift keying (BPSK) modulation is obtained when $a = 1$ and $b = 2$, while that for the M-ary Pulse Amplitude Modulation (M-PAM), $a = 2(M-1)/M$ and $b = 6/(M^2-1)$. In the same way, $a = b = 2$ are applied for the average SER of the quadrature phase shift keying (QPSK) modulation. Finally, $a = 2$ and $b = 2\sin^2(\pi/M)$ for M-ary phase shift keying (M-PSK) modulation, while $a = 4(1 - 1/\sqrt{M})$ and $b = 3/(M-1)$ for the average SER of the M-ary quadrature amplitude modulation (M-QAM), when $M > 4$.

$$\begin{aligned} C_{\text{upper}}^{\text{max.}} &= \lim_{Q \to \infty} C_{\text{upper}} \\ &= \lim_{Q \to \infty} \log_2\left(1 + N\rho\beta_g\beta_h\left[1 + \frac{1}{16}(N-1)Q^2\sin^2\left(\frac{\pi}{Q}\right)\right]\right) \\ &= \log_2\left(1 + N\rho\beta_g\beta_h\left[1 + \frac{(N-1)\pi^2}{16}\right]\right). \end{aligned} \tag{28}$$

$$\begin{aligned} C_{\text{lower}}^{\text{max.}} &= \lim_{Q \to \infty} C_{\text{lower}} \\ &= \log_2\left(1 + \frac{N^2\rho\beta_g\beta_h\left(\pi^2(N-1)+16\right)^3}{16\left((N-1)\left(\pi^4\left(N^2-5N+6\right)+48\pi^2(2N-1)+256\right)+512(N+1)\right)}\right). \end{aligned} \tag{29}$$

Remark 11: In high SNR regime, the average SER can be approximated as

$$P_e^{\text{high-SNR}} \approx a 2^{-\frac{\kappa}{2}-1} b^{-\frac{\kappa}{2}} \theta^{-\kappa} \left(\frac{1}{\Gamma\left(\frac{\kappa}{2}+1\right)} - \frac{\kappa}{\sqrt{2b}\theta\Gamma\left(\frac{\kappa+3}{2}\right)} \right), \tag{42}$$

whose proof is provided in Appendix J.

After analyzing (42), it is possible to observe that the first term inside the parentheses is the dominant one. Otherwise, the average SER would be a negative number since a, b, and θ are values greater than zero. This direct insight results in the following remark.

Remark 12: The average SER decreases when κ and/or b increases and when a and/or θ decreases.

As shown in Section IV, this remark demonstrates that the average SER decreases as the transmission power, ρ, the number of reflecting elements, N, and/or the number of quantization levels, Q, increase. On the other hand, the average SER increases as the modulation order increases.

F. DIVERSITY ORDER

The diversity order is a fundamental parameter of diversity-based systems. It measures the number of independent paths over which the data is received. The diversity order, D, is formally defined as the negative slope of the average SER versus the average SNR curve in a log-log scale and calculated as by [57]

$$D = \lim_{\rho \to \infty} -\frac{\log P_e}{\log \rho}. \tag{43}$$

From the definition above, we can see that the diversity order is a high-SNR concept.

Remark 13: The diversity order of the LIS-assisted system is obtained as

$$D = \frac{5\mathcal{A}_1^2 + \sqrt{49\mathcal{A}_1^4 - 34\mathcal{A}_1^2\mathcal{A}_2 + \mathcal{A}_2^2} - \mathcal{A}_2}{4\left(\mathcal{A}_2 - \mathcal{A}_1^2\right)}. \tag{44}$$

The parameters and proof of (44) are detailed in Appendix K. From them, we realize that the diversity order increases with N.

Remark 14: Despite both source and destination being equipped with a single antenna, the achievable diversity order grows with the number of LIS reflecting elements. It is worth noting that each reflecting element modifies the incident waves' phases to add at the destination coherently. A direct SISO path between source and destination would only allow for a unitary diversity order, once diversity gains can only be obtained by employing multiple antennas at transmission and/or receiving sides. However, LIS employment provides a substantial diversity order to the communication system just by adding passive reflecting elements with adjustable phases to the system.

G. POWER-SCALING LAW

This subsection analyses the power-scaling law of the ergodic spectral efficiency regarding the number of reflecting elements in an LIS-assisted system in which $N \to \infty$.

If N grows without limit and we consider that the transmit power, ρ, can be scaled down with N^2 according $\rho = P/N^2$ and P is fixed, then (25) and (28) become, respectively

$$\begin{aligned} C_{\text{upper}} &= \log_2\left(1 + N\frac{P}{N^2}\beta_g\beta_h\left[1 + \frac{(N-1)Q^2\sin^2\left(\frac{\pi}{Q}\right)}{16}\right]\right) \\ &\to \frac{P\beta_g\beta_h Q^2\sin^2\left(\frac{\pi}{Q}\right)}{16}, N \to \infty \end{aligned} \tag{45}$$

and

$$\begin{aligned} C_{\text{upper}}^{\text{max.}} &= \log_2\left(1 + N\frac{P}{N^2}\beta_g\beta_h\left[1 + \frac{(N-1)\pi^2}{16}\right]\right) \\ &\to \frac{P\beta_g\beta_h\pi^2}{16}, N \to \infty. \end{aligned} \tag{46}$$

These results confirm that with many reflecting elements and perfect channel information, the transmit power can be reduced proportionally to $1/N^2$ without compromising the spectral efficiency.

Remark 15: From (25) and (45), it is possible to see that if we decrease the transmit power proportionally to $1/N^\alpha$, with $\alpha > 2$, then the SNR goes to zero as $N \to \infty$. When $\alpha < 2$, the SNR grows without bound as $N \to \infty$. This means that $1/N^2$ (i.e., $\alpha = 2$) is the fastest rate at which we can decrease the transmit power and still maintain a fixed rate.

The Remark 15 shows that as N grows without bound, the transmit power can be reduced proportionally to $1/N^2$. The transmit power reduction is significant mainly to power-constrained devices such as the Internet of Things (IoT) devices [58], [59].

IV. SIMULATION RESULTS

This section presents numerical results to validate the derived expressions against Monte Carlo simulations obtained from 10^6 realizations. The setup in Figure 2 shows the geometric placement adopted for the BS, LIS and UE, where r_g and r_h are the distances between source (*i.e.*, the BS) and LIS, and between LIS and destination (*i.e.*, the UE), respectively. Both of them are set to 25 m.

$$P_e = \mathbb{E}\left[a\mathcal{Q}\left(\sqrt{b\gamma}\right)\right] = a2^{-\frac{\kappa}{2}-1} b^{-\frac{\kappa}{2}} \theta^{-\kappa} \left(\frac{{}_2F_2\left(\frac{\kappa}{2}+\frac{1}{2}, \frac{\kappa}{2}; \frac{1}{2}, \frac{\kappa}{2}+1; \frac{1}{2b\theta^2}\right)}{\Gamma\left(\frac{\kappa}{2}+1\right)} - \frac{\kappa\, {}_2F_2\left(\frac{\kappa}{2}+\frac{1}{2}, \frac{\kappa}{2}+1; \frac{3}{2}, \frac{\kappa}{2}+\frac{3}{2}; \frac{1}{2b\theta^2}\right)}{\sqrt{2b}\theta\Gamma\left(\frac{\kappa+3}{2}\right)} \right). \tag{41}$$

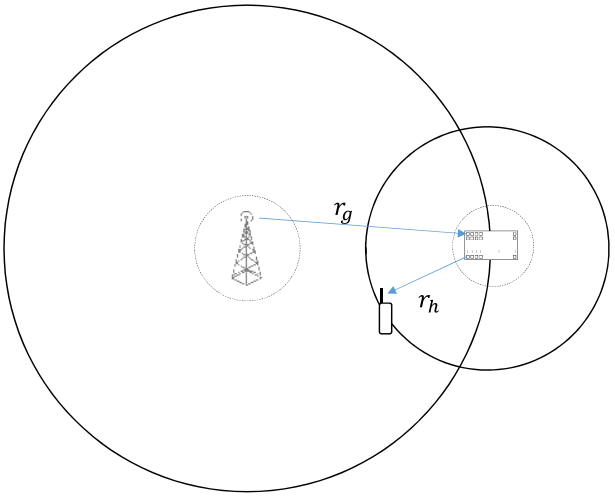

FIGURE 2. Adopted simulation setup.

We assume that the large-scale fading coefficients are modeled as $\beta_g = z_g/(r_g)^v$ and $\beta_h = z_h/(r_h)^v$, in which z_g and z_h are log-normal random variables with standard deviation σ_{shadow}, while r_g is the distance between the source and the LIS and r_h is the distance between the LIS and the destination. v is the path-loss exponent. For all simulation results, we adopt the typical suburban area parameters $\sigma_{\text{shadow}} = 8$ dB and $v = 3.67$.

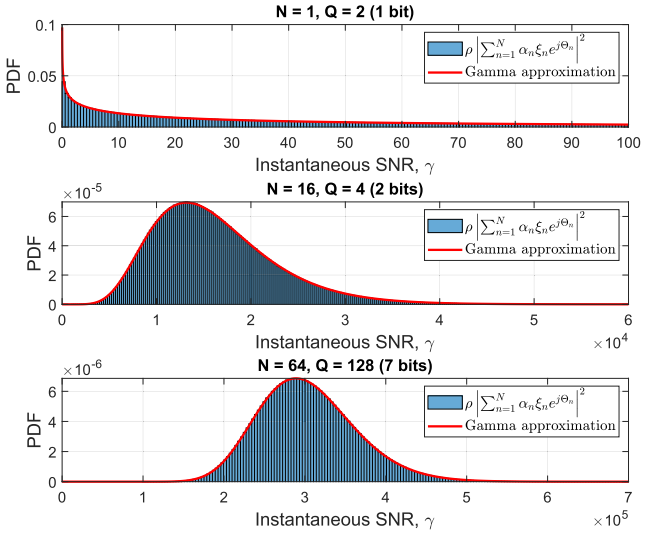

FIGURE 3. Comparison of the approximated PDF for the instantaneous sum-capacity.

Figure 3 presents some comparisons of the normalized histogram of the random variable given by the instantaneous SNR (see (5)) against the theoretical PDF given by (11). As can be noticed, even for a small number of reflecting elements and quantization bits, the approximation is quite tight.

Figure 4 shows the Kullback-Leibler Divergence [60] between the approximated SNR PDF and the real distribution of the SNR random variable over the variation of the number of quantization bits and for several values of LIS elements, N. In general, this is the most known technique to evaluate an approximation in statistics. As can be seen, from $b = 2$ bits onward, the divergence remains constant regardless of the number of elements. Additionally, the figure also shows that as the number of elements increases, the divergence decreases. These results reveal that only the number of LIS reflecting elements can take the approximated PDF closer to the real one and that the number of quantization bits has a minimal impact on it. It is aligned to the theory since an inspection of (6) reveals that only the number of reflecting elements impact the summation in that equation.

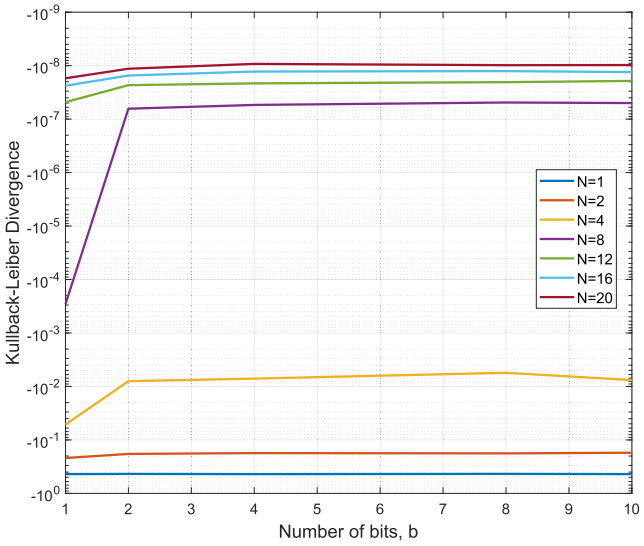

FIGURE 4. Kullback-Leibler divergence between the approximated SNR PDF and the real distribution.

From Figure 5, which shows the spectral efficiency as a function of N for $b \in \{1, 4, 10\}$, we can see that the accuracy of the approximation becomes better not only as N increases but also when more bits are dedicated to phase quantization. For comparison, we also present the simulated capacity curve of a SISO system without the assistance of an LIS. When $b = 1$, the aid provided by an LIS becomes advantageous for $N > 80$. Otherwise, When $b > 1$, an LIS with $N > 50$ is enough for the LIS-assisted system's behavior to outperform that of the system without an LIS.

We also verify the performance degradation when b varies. As shown in Figure 6, the spectral efficiency decreases when b is small. This is evident, especially for $b = 1$ and $b = 2$. Therefore, the performance difference between the spectral efficiency obtained when using perfect phase shifts and quantized phase shifts decreases as b increases. Moreover, the degradation also tends to decrease as more reflective

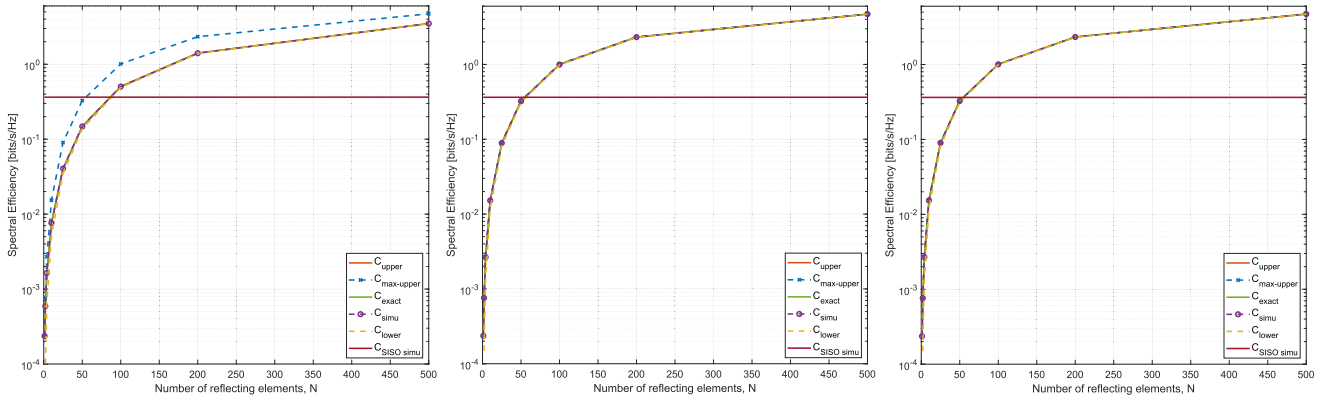

FIGURE 5. Spectral efficiency as a function of N for (a) $b = 1$ (b) $b = 4$ (c) $b = 10$.

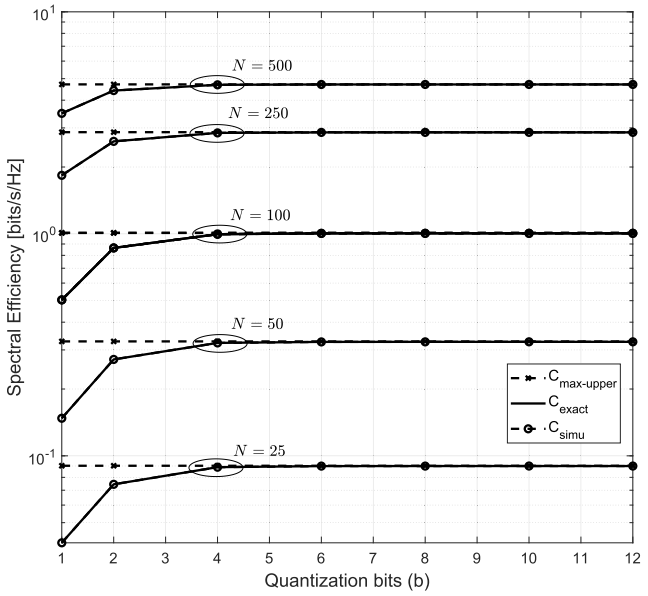

FIGURE 6. Spectral efficiency as a function of b for different values of N.

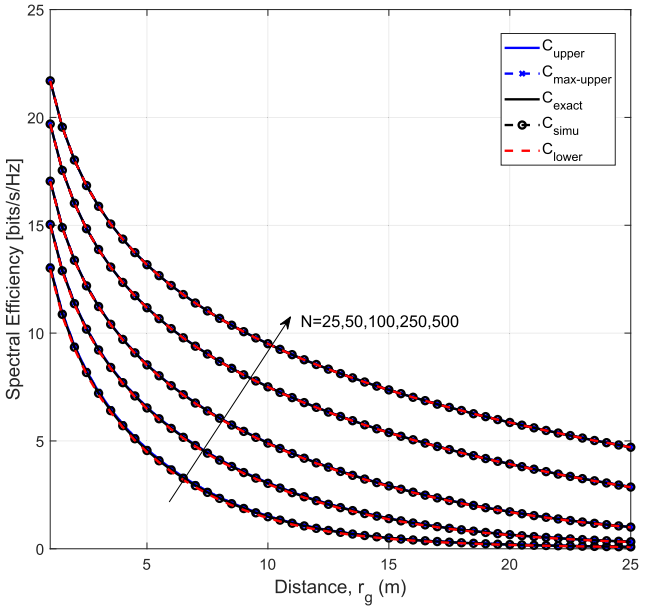

FIGURE 7. Spectral efficiency as a function of the distance between source and LIS, considering $b = 8$.

elements are added to the LIS. That is, for an LIS with many elements, a few bits (as few as 4 bits) are sufficient for quantization with negligible performance degradation, which is in accordance (28).

Regarding the distance between the source (*i.e.*, the BS) and the LIS, we compare the schemes' spectral efficiencies with $N = 25, 50, 100, 250, 500$. Figure 7 shows the results obtained for $b = 8$. We can see that the performance deteriorates as the distance increases. This phenomenon was expected since the LIS is composed of only passive elements and there is no direct path between the source and the user. However, as already mentioned, it improves when the number of elements on LIS increases.

In its turn, Figure 8 shows how the spectral efficiency behaves as $\rho = P/N^{\alpha}$ varies for $\alpha = 3/2, 2, 5/2$. We consider $P = 100$ [dB] and $b \in \{1, 2, 4, 8, 10\}$. As expected and stated in Remark 15, for $\alpha = 2$ and as N increases, the capacity becomes constant no matter the number of reflecting elements. However, when $\alpha = 3/2$, the capacity grows logarithmically fast with N when $N \to \infty$ and tends to 0 when $\alpha = 5/2$ and $N \to \infty$. These results confirm that the transmit power can be reduced proportionally to N. We can also see that, although the capacity increases with the number of quantization bits, b, the performances for $b = 4$, $b = 8$, and $b = 10$ are very close.

Figure 9 shows the required transmit power by the source needed to achieve fixed capacities of 1 and 2 bits/s/Hz, respectively. As expected and predicted by Remark 15, the transmit power can be reduced by approximately 6 [dB] by doubling the number of reflecting elements for both fixed capacities. We can also confirm that, in general,

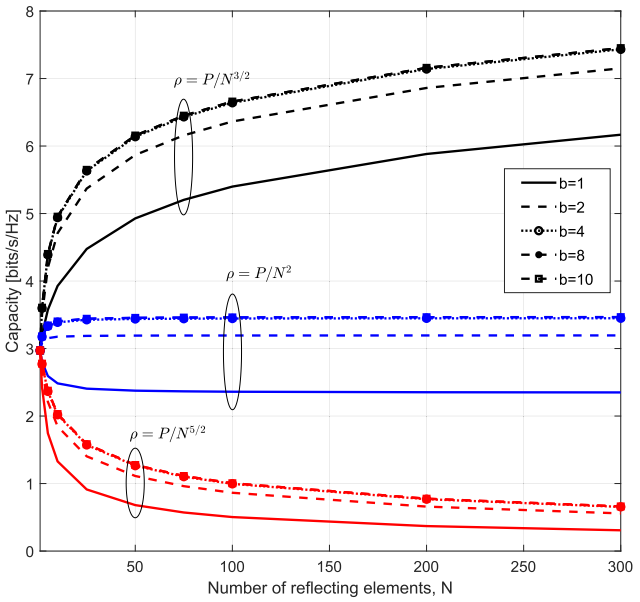

FIGURE 8. Power scaling law for different α values.

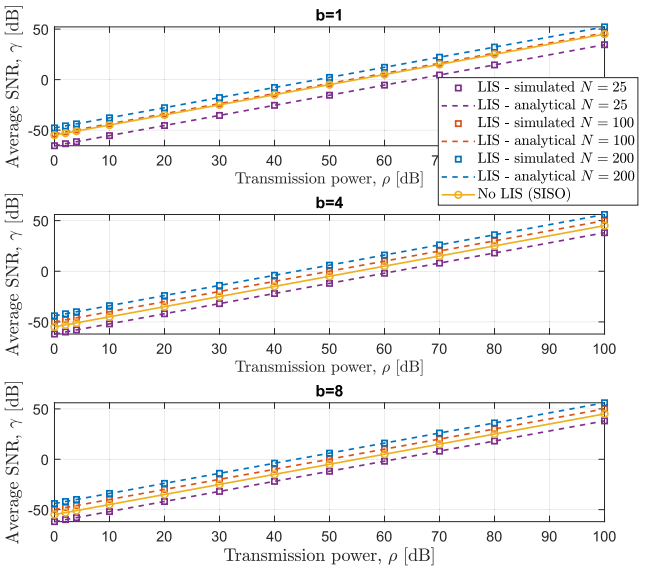

FIGURE 10. Average SNR in function of transmission power for $b = 1$, $b = 4$ and $b = 8$.

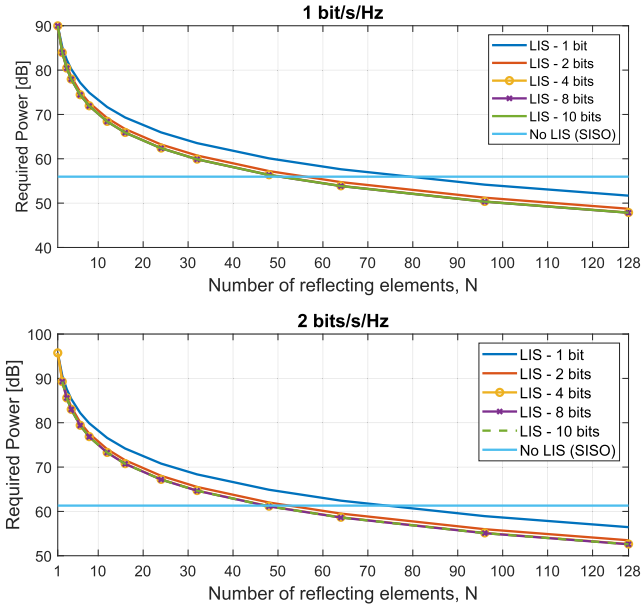

FIGURE 9. Required power for $C = 1$ bit/s/Hz and $C = 2$ bits/s/Hz.

the LIS-assisted system outperforms the SISO system without LIS when N is approximately greater than 80, regardless of the number of quantization bits.

Figure 10 compares the average SNR as a function of the transmitted power obtained from the simulations, (9), and the SISO system without LIS. We consider $\rho = 50$ dB, $N \in \{25, 100, 200\}$ and $b \in \{1, 4, 8\}$. As can be confirmed, the relationship between the two parameters is linear, *i.e.*, between the average SNR and the transmitted power. Additionally, we can notice that, for a given ρ, the average SNR improves as N increases. It is also worth mentioning that the LIS-assisted system outperforms the conventional one the higher the number of reflecting elements N is. Moreover, the influence of the number of quantization bits is insignificant, as long as $b > 1$.

Figures 11 and 12 show the symbol error rate behavior for BPSK and QPSK, and 16-QAM, and 64-QAM modulation schemes considering $N = 25$, respectively. As expected, the modulations present a decreasing level of robustness as the number of symbols increases. The most important thing to note here is the gap between the curves for 1, 2, and 4 bits. It gets to be almost 5 dB when the SNR is high. Although this gap exists, it is less pronounced when more bits are dedicated

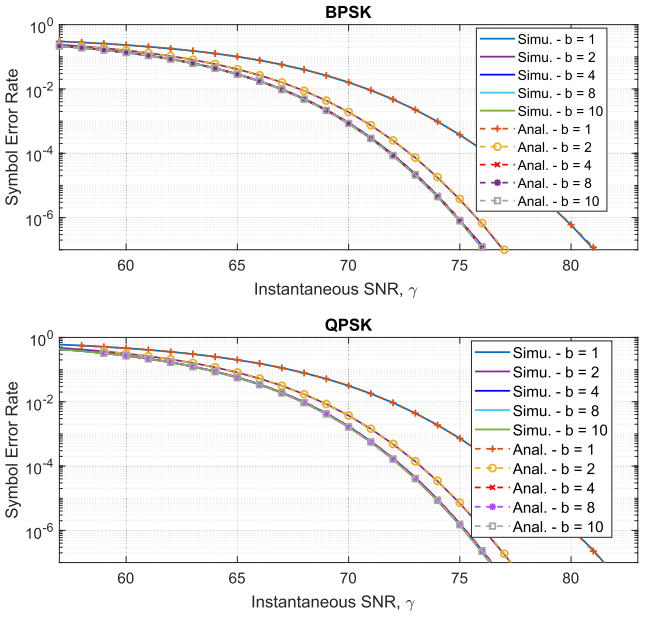

FIGURE 11. Symbol Error Rate for BPSK and QPSK modulations for $N = 25$.

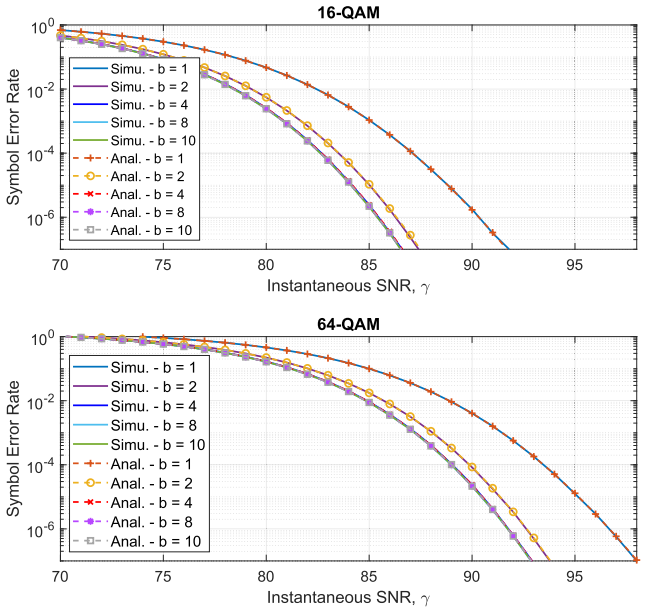

FIGURE 12. Symbol Error Rate for 16-QAM and 64-QAM modulations for $N = 25$.

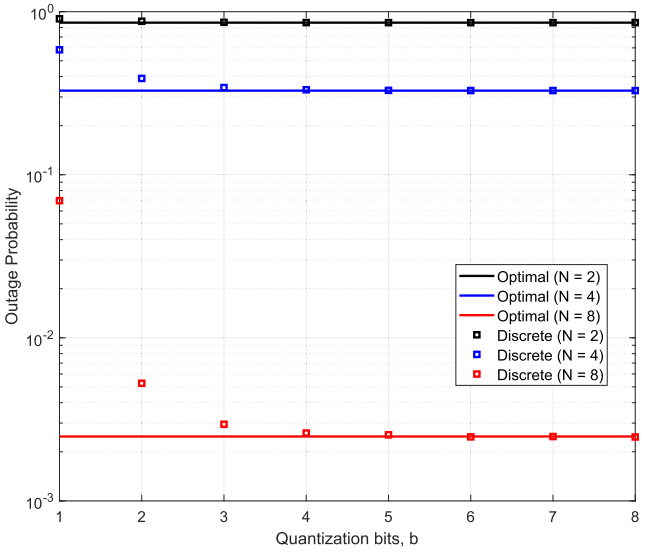

FIGURE 14. Outage probability versus number of quantization bits, b, for different values of N.

to phase quantization, and $b = 4$ is enough to guarantee a good performance.

For computational simplicity, in Figure 13, we present the simulated and analytical outage probabilities only for $N = 100$. We notice that the probability of achieving higher capacities increases with the number of quantization bits, b. Moreover, when considering different b values, we can confirm the previous insight; $b = 4$ is enough for a good phase quantization.

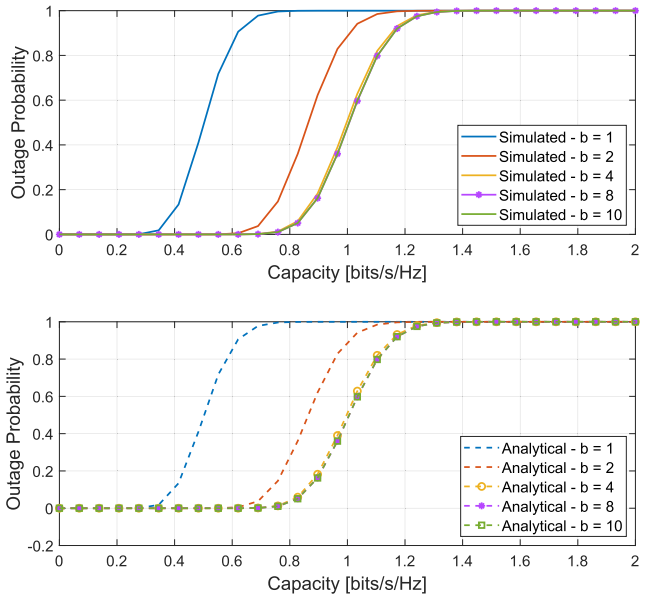

FIGURE 13. Outage probability for $N = 100$ and $b \in \{1, 2, 4, 8, 10\}$.

Finally, Figure 14 shows the outage probability as we vary the number of quantization bits. For this simulation, we assume ρ equal to 80 [dB] and the capacity of 1 bit/s/Hz. By analyzing the results, it is possible to notice that the outage probability decreases as the number of quantization bits, b, increases and asymptotically approaches the lower bound given by an optimal LIS with perfect phase shifts, *i.e.*, an infinite number of bits used to represent the phases. For all the three setups, $N = 2$, 4, and 8, the outage probability reaches its largest value when $b = 2$. When $N = 2$, the outage probability approaches the perfect phase bound as long as $b > 3$. We also notice that the gap between the curves gets larger as N increases. However, it reduces as the number of quantization bits, b, increases. Therefore, we conclude that the phase quantization errors do not significantly impact the outage probability performance as long as the number of bits is made large enough, which is an encouraging finding for the deployment of LIS-assisted systems.

V. CONCLUSION AND FUTURE WORK

In this article, we have done an in-depth analysis of a practical LIS-assisted SISO system. Since quantization errors are unavoidable, we have evaluated the influence of bits number dedicated to the phase quantization on spectral efficiency, symbol error rate, and outage probability. We have compared such a system performance with the conventional one without LIS through accurate closed-form expressions derived for each of these metrics. We have extended our analysis to power scaling law and the power required to achieve specific capacity. Not only is the influence of b verified, but also that of the number of LIS elements.

We can conclude that the system's performance improves as the numbers of LIS elements and bits increase. With approximately fifty reflecting elements and four dedicated bits for phase quantization, the LIS-assisted system outperforms the conventional system performance without a LIS.

Our study assumed that (i) there is no direct link between S and D, and (ii) the intermediate channels (*i.e.*, S to LIS and LIS to D) are independent, flat, and Rayleigh distributed. As future work, we intend to relax those assumptions and study the performance of LIS-assisted systems with discrete phase sets in correlated fading channels with the presence and absence of direct links between the involved entities (*i.e.*, S, LIS, and D).

APPENDIX A

To find the parameters κ and θ for the approximated PDF of λ, we first need to define the following Lemmas.

Lemma 2:

$$\left|\sum_{n=1}^{N} z_n e^{j\theta_n}\right|^2 = \sum_{n=1}^{N} z_n^2 + 2\sum_{m=1}^{N}\sum_{n=m+1}^{N} z_m z_n \cos(\theta_m - \theta_n). \tag{47}$$

Proof: This identity is straightforwardly found by expanding the summation terms on its left side. □

Lemma 3: If $X \sim \mathcal{CN}(0_M, \sigma_X^2 I_M)$, then $Y = |X|$ is a Rayleigh random variable with PDF given by

$$f_Y(y) = \frac{2y}{\sigma_X^2} e^{-\frac{y^2}{\sigma_X^2}}, y \geq 0. \tag{48}$$

Proof: The proof for this Lemma is given in [61]. □

Lemma 4: If Y is a Rayleigh random variable with PDF defined by (48)*, then, its 4 first moments are given by*

$$\mathbb{E}[Y] = \int_0^\infty y f_Y(y) dy = \frac{\sigma_X\sqrt{\pi}}{2}, \tag{49}$$

$$\mathbb{E}\left[Y^2\right] = \int_0^\infty y^2 f_Y(y) dy = \sigma_X^2, \tag{50}$$

$$\mathbb{E}\left[Y^3\right] = \int_0^\infty y^3 f_Y(y) dy = \frac{3\sigma_X^3\sqrt{\pi}}{4}, \tag{51}$$

$$\mathbb{E}\left[Y^4\right] = \int_0^\infty y^4 f_Y(y) dy = 2\sigma_X^4. \tag{52}$$

Lemma 5: If X is a uniform random variable with PDF given by

$$f_X(x) = \begin{cases} \frac{a}{2\pi}, & -\frac{\pi}{a} \leq x \leq \frac{\pi}{a}, \\ 0, & otherwise, \end{cases} \tag{53}$$

then $Y = -X$ has the same PDF as X, which was defined in (53)*.*

Proof: This can be straightforwardly proved by noticing that the PDF of X is symmetrical around 0. □

Lemma 6: If θ_m and θ_n are independent and identically distributed uniform random variables with PDF given by (53)*, then $Y = \theta_m + \theta_n$ has the following PDF*

$$f_Y(y) = \begin{cases} \frac{a}{2\pi}\left(1 + \frac{a}{2\pi}y\right), & -\frac{2\pi}{a} \leq y \leq 0, \\ \frac{a}{2\pi}\left(1 - \frac{a}{2\pi}y\right), & 0 < y \leq \frac{2\pi}{a}, \\ 0, & otherwise. \end{cases} \tag{54}$$

Proof: From the theory, we know that the sum of two random variables equals the convolution of $f_{\theta_m}(\theta_m)$ and $f_{\theta_n}(\theta_n)$ is

$$f_Y(y) = \int_{-\infty}^{\infty} f_{\theta_m}(y - \theta_n) f_{\theta_n}(\theta_n) d\theta_n. \tag{55}$$

Therefore, $f_Y(y)$ is defined as

$$f_Y(y) = \begin{cases} \int_{-\frac{\pi}{a}}^{\frac{\pi}{a}+y} \frac{a^2}{4\pi^2} d\theta_n, & -\frac{2\pi}{a} \leq y < 0, \\ \int_{-\frac{\pi}{a}+y}^{\frac{\pi}{a}} \frac{\beta_g}{4\pi^2} d\theta_n, & 0 \leq y \leq \frac{2\pi}{a}, \\ 0, & otherwise, \end{cases} \tag{56}$$

which concludes the proof. □

Lemma 7: If the PDF of the sum of two independent and identically distributed uniform random variables is given by (54)*, then*

$$\mathbb{E}[\cos(\theta_m - \theta_n)] = \frac{a^2 \sin^2(\frac{\pi}{a})}{\pi^2}. \tag{57}$$

Proof: By using Lemma 5, we can rewrite (57) as $\mathbb{E}[\cos(\theta_m + \theta_n)]$, then applying Lemma 6 we have

$$\begin{aligned} \mathbb{E}[\cos(\theta_m + \theta_n)] &= \mathbb{E}[\cos(y)] \\ &= \int_{-\frac{2\pi}{a}}^{0} \cos(y)\frac{a}{2\pi}\left(1 + \frac{a}{2\pi}y\right) dy \\ &\quad + \int_{-\frac{2\pi}{a}}^{0} \cos(y)\frac{a}{2\pi}\left(1 - \frac{a}{2\pi}y\right) dy. \end{aligned} \tag{58}$$

Solving the two integrals in (58) concludes the proof. □

Lemma 8: If the PDF of the sum of two independent and identically distributed uniform random variables is given by (54)*, then*

$$\mathbb{E}\left[\cos^2(\theta_m - \theta_n)\right] = \frac{8\pi^2 + a^2 - a^2\cos^2(\frac{4\pi}{a})}{16\pi^2}. \tag{59}$$

Proof: By using Lemma 5 we can rewrite (57) as $\mathbb{E}\left[\cos^2(\theta_m + \theta_n)\right]$, then applying Lemma 6 we have

$$\begin{aligned} \mathbb{E}\left[\cos^2(\theta_m + \theta_n)\right] &= \mathbb{E}\left[\cos^2(y)\right] \\ &= \int_{-\frac{2\pi}{a}}^{0} \cos^2(y)\frac{a}{2\pi}\left(1 + \frac{a}{2\pi}y\right) dy \\ &\quad + \int_{-\frac{2\pi}{a}}^{0} \cos^2(y)\frac{a}{2\pi}\left(1 - \frac{a}{2\pi}y\right) dy. \end{aligned} \tag{60}$$

Solving the two integrals in (60) concludes the proof. □

Lemma 9: If X is a uniform random variable with PDF given by (53)*, then the PDF of $Y = 2X$ is given by*

$$f_Y(y) = \frac{a}{4\pi}, -\frac{2\pi}{a} \leq y \leq \frac{2\pi}{a}. \tag{61}$$

Proof: This is proved by using the standard transformation of random variables. □

Lemma 10: If θ_l, θ_m and θ_n are independent and identically distributed uniform random variables with PDF given by (53), then $Y = 2\theta_l - (\theta_m + \theta_n)$ has the following PDF

$$f_Y(y) = \begin{cases} \frac{a}{2\pi} + \frac{a^2 y}{4\pi^2} + \frac{a^3 y^2}{32\pi^3}, & -\frac{4\pi}{a} \leq y \leq -\frac{2\pi}{a}, \\ \frac{a}{4\pi} - \frac{a^3 y^2}{32\pi^3}, & -\frac{2\pi}{a} < y \leq 0, \\ \frac{a}{4\pi} - \frac{a^3 y^2}{32\pi^3}, & 0 < y \leq \frac{2\pi}{a}, \\ \frac{a}{2\pi} - \frac{a^2 y}{4\pi^2} + \frac{a^3 y^2}{32\pi^3}, & \frac{2\pi}{a} < y \leq \frac{4\pi}{a}, \\ 0, & \text{otherwise}. \end{cases} \tag{62}$$

Proof: We start by remembering that we know the PDF of $W = 2\theta_l$ and of $Z = \theta_m + \theta_n$, which are given by (61) and (54), respectively. Next by applying Lemma 5, we can re-write Y as $Y = Z + W$, which is the sum of two independent random variables. Therefore, the PDF of Y is the convolution between the PDFs of W and Z, which is defined as

$$f_Y(y) = \int_{-\infty}^{\infty} f_W(y - z) f_Z(z) dz. \tag{63}$$

Therefore, $f_Y(y)$ is defined as

$$f_Y(y) = \begin{cases} \int_{-\frac{2\pi}{a}}^{\frac{2\pi}{a}+y} \frac{a^2}{8\pi^2}\left(1 + \frac{a}{2\pi}z\right) dz, \\ \quad -\frac{4\pi}{a} \leq y < -\frac{2\pi}{a}, \\ \int_{0}^{\frac{2\pi}{a}+y} \frac{a^2}{8\pi^2}\left(1 - \frac{a}{2\pi}z\right) dz + \int_{-\frac{\pi}{a}+y}^{\frac{\pi}{a}} \frac{a^2}{8\pi^2}\left(1 + \frac{a}{2\pi}z\right) dz, \\ \quad -\frac{2\pi}{a} \leq y < 0, \\ \int_{-\frac{2\pi}{a}+y}^{0} \frac{a^2}{8\pi^2}\left(1 + \frac{a}{2\pi}z\right) dz + \int_{-\frac{\pi}{a}+y}^{\frac{\pi}{a}} \frac{a^2}{8\pi^2}\left(1 - \frac{a}{2\pi}z\right) dz, \\ \quad 0 \leq y < \frac{2\pi}{a}, \\ \int_{-\frac{2\pi}{a}+y}^{\frac{2\pi}{a}} \frac{a^2}{8\pi^2}\left(1 - \frac{a}{2\pi}z\right) dz, \\ \quad \frac{2\pi}{a} \leq y \leq \frac{4\pi}{a}, \\ 0, \quad \text{otherwise}, \end{cases} \tag{64}$$

which concludes the proof. □

Lemma 11: If the PDF of the sum of three independent random variables, $Y = 2\theta_l - (\theta_m + \theta_n)$, is given by (62), then

$$\mathbb{E}\left[\cos(2\theta_l - (\theta_m + \theta_n))\right] = \frac{a^3 \cos(\frac{\pi}{a}) \sin^3(\frac{\pi}{a})}{\pi^3}. \tag{65}$$

Proof: By using Lemma 10 we have

$$\begin{aligned} &\mathbb{E}\left[\cos(2\theta_l - (\theta_m + \theta_n))\right] \\ &\quad = \mathbb{E}\left[\cos(y)\right] \\ &\quad = \int_{-\frac{4\pi}{a}}^{-\frac{2\pi}{a}} \cos(y)\left[\frac{a}{2\pi} + \frac{a^2 y}{4\pi^2} + \frac{a^3 y^2}{32\pi^3}\right] dy \\ &\quad + \int_{-\frac{2\pi}{a}}^{\frac{2\pi}{a}} \cos(y)\left[\frac{a}{4\pi} - \frac{a^3 y^2}{32\pi^3}\right] dy \\ &\quad + \int_{\frac{2\pi}{a}}^{\frac{4\pi}{a}} \cos(y)\left[\frac{a}{2\pi} - \frac{a^2 y}{4\pi^2} + \frac{a^3 y^2}{32\pi^3}\right] dy. \end{aligned} \tag{66}$$

Solving the three integrals in (66) concludes the proof. □

Lemma 12: If θ_l, θ_m, and θ_n are independent and identically distributed uniform random variables with PDF given by (53), then

$$\mathbb{E}[\cos(\theta_l - \theta_m)\cos(\theta_l - \theta_n)] = \frac{a^2 \sin^2(\frac{\pi}{a})\left[2\pi + a\sin(\frac{2\pi}{a})\right]}{4\pi^3}. \tag{67}$$

Proof: We start by applying the trigonometric identity $\cos(a)\cos(b) = \frac{\cos(a-b)+\cos(a+b)}{2}$ to (68), which then can be re-written as

$$\begin{aligned} \mathbb{E}\left[\cos(\theta_l - \theta_m)\cos(\theta_l - \theta_n)\right] &= \frac{1}{2}\mathbb{E}\left[\cos(\theta_n - \theta_m)\right] \\ &\quad + \frac{1}{2}\mathbb{E}\left[\cos(2\theta_l - \theta_n - \theta_m)\right]. \end{aligned} \tag{68}$$

Next, by applying Lemmas 7 and 11 to (68), we conclude the proof.

□

A. APPROXIMATED PDF OF THE INSTANTANEOUS SNR

Let the random variable $Z = r$, where r is defined in (6), therefore, the PDF of Z can be accurately approximated by a Gamma distribution with parameters κ and θ, defined by (7) and (8), respectively. This is empirically proven by comparing the normalized histogram of Z against the theoretical PDF of a Gamma random variable, Y, with the parameters defined earlier.

In order to approximate Z as a Gamma random variable, Y, we have to find the parameters shape and scale (*i.e.*, κ and θ) based on statistical information of Z. Therefore, we approximate Z as a Gamma random variable, Y, by using two different moments of Y and then assuming that $\mathbb{E}\left[Y^2\right] = \mathbb{E}\left[Z^2\right]$ and $\mathbb{E}\left[Y^4\right] = \mathbb{E}\left[Z^4\right]$.

Those two moments of the Gamma distribution Y are defined as

$$\mathbb{E}\left[Y^2\right] = \kappa(\kappa + 1)\theta^2, \tag{69}$$

and

$$\mathbb{E}\left[Y^4\right] = \kappa(\kappa + 1)(\kappa + 2)(\kappa + 3)\theta^4. \tag{70}$$

Based on (69), the assumption that $\mathbb{E}\left[Y^2\right] = \mathbb{E}\left[Z^2\right]$ and then isolating θ we find

$$\theta = \sqrt{\frac{\mathbb{E}\left[Z^2\right]}{\kappa(\kappa + 1)}}. \tag{71}$$

Next, plugging (71) back into (70) and assuming that $\mathbb{E}\left[Y^4\right] = \mathbb{E}\left[Z^4\right]$, we find κ as

$$\left(\mathbb{E}\left[Z^4\right]-\mathbb{E}\left[Z^2\right]^2\right)\kappa^2+\left(\mathbb{E}\left[Z^4\right]-5\mathbb{E}\left[Z^2\right]^2\right)\kappa-6\mathbb{E}\left[Z^2\right]^2=0, \tag{72}$$

which is a quadratic equation with the following two roots

$$\kappa_0 = \frac{-\left(\mathbb{E}[Z^4]-5\mathbb{E}[Z^2]^2\right)+\sqrt{\mathbb{E}[Z^4]^2-34\mathbb{E}[Z^4]\mathbb{E}[Z^2]^2+49\mathbb{E}[Z^2]^4}}{2\left(\mathbb{E}\left[Z^4\right]-\mathbb{E}\left[Z^2\right]^2\right)}, \tag{73}$$

$$\kappa_1 = \frac{-\left(\mathbb{E}[Z^4]-5\mathbb{E}[Z^2]^2\right)-\sqrt{\mathbb{E}[Z^4]^2-34\mathbb{E}[Z^4]\mathbb{E}[Z^2]^2+49\mathbb{E}[Z^2]^4}}{2\left(\mathbb{E}\left[Z^4\right]-\mathbb{E}\left[Z^2\right]^2\right)}, \tag{74}$$

where out of the two roots, only is useful, *i.e.*, only one root has a positive value. Since κ ought to be a real and positive number, we assume that the value within the square root is a positive one. Next, assuming that $5\mathbb{E}\left[Z^2\right]^2 \geq \mathbb{E}\left[Z^4\right]$, then only κ_0 results in a positive value.

Next, in order to find the moment $\mathbb{E}\left[Z^2\right]$, we first expand $\mathbb{E}\left[Z^2\right]$ as

$$\begin{aligned}\mathbb{E}\left[Z^2\right] &= \mathbb{E}\left[\gamma\right] \\ &= \mathbb{E}\left[\rho\left|\sum_{n=1}^{N}|h_n||g_n|e^{j\delta_n}\right|^2\right] \\ &= \mathbb{E}\left[\rho\sum_{n=1}^{N}d_n^2+2\rho\sum_{m=1}^{N}\sum_{n=m+1}^{N}d_m d_n\cos(\delta_m-\delta_n)\right],\end{aligned} \tag{75}$$

where $d_k = |h_k||g_k|$ and the last line is found by applying Lemma 2. Thus, using the fact that $|h_n|$, $|g_n|$, and δ_n, $\forall n$ are mutually independent random variables and that h_m and h_n, and g_m and g_n, $\forall m, n$ are identically distributed, then (75), can be re-written as

$$\begin{aligned}\mathbb{E}\left[Z^2\right] &= \rho\sum_{n=1}^{N}\mathbb{E}\left[|h_n|^2\right]\mathbb{E}\left[|g_n|^2\right] \\ &\quad+2\rho\sum_{m=1}^{N}\sum_{n=m+1}^{N}\mathbb{E}\left[|h_m|\right]^2\mathbb{E}\left[|g_m|\right]^2\mathbb{E}\left[\cos(\delta_m-\delta_n)\right].\end{aligned} \tag{76}$$

Then, by applying Lemmas 4 and 7 to (76), we find (9).

Next, in order to find the moment $\mathbb{E}\left[Z^4\right]$, we initially expand it as

$$\begin{aligned}\mathbb{E}\left[Z^4\right] &= \mathbb{E}\left[\gamma^2\right] \\ &= \mathbb{E}\left[\left(\sum_{l=1}^{N}d_l^2\right)^2\right] \\ &\quad+4\sum_{l=1}^{N}\sum_{m=1}^{N}\sum_{n=m+1}^{N}\mathbb{E}\left[d_l^2 d_m d_n\cos(\delta_m-\delta_n)\right] \\ &\quad+4\mathbb{E}\left[\left(\sum_{m=1}^{N}\sum_{n=m+1}^{N}d_m d_n\cos(\delta_m-\delta_n)\right)^2\right],\end{aligned} \tag{77}$$

where $d_k = |h_k||g_k|$. The first term of (77) can be expressed as

$$\begin{aligned}\mathbb{E}\left[\left(\sum_{l=1}^{N}d_l^2\right)^2\right] &= \mathbb{E}\left[\sum_{n=1}^{N}d_n^4+\sum_{m=1}^{N}\sum_{n=1,n\neq m}^{N}d_m^2 d_n^2\right] \\ &= N\mathbb{E}\left[|g_m|^4\right]\mathbb{E}\left[|h_m|^4\right] \\ &\quad+N(N-1)\mathbb{E}\left[|g_m|^2\right]^2\mathbb{E}\left[|h_m|^2\right]^2 \\ &= N(N+3)\left(\beta_g\beta_h\right)^2,\end{aligned} \tag{78}$$

where the last line of (78) is found by applying Lemma 4. Next, the second term of (77) can be expressed as (79), as shown at the bottom of the next page, where the last line is found by applying Lemmas 4 and 7. Then, the third term of (77) can be expressed as (80), as shown at the bottom of the next page, where the last line is found after applying Lemmas 4, 7, 8, and 12. Finally, after plugging (78), (79), and (80) back into (77) and several simplifications, we find (10).

The proof is concluded by replacing Equations (9) and (10) into the definitions of κ and θ, given by (73) and (71), respectively.

APPENDIX B

For the derivation of Remark 1, we need to define the following Lemma.

Lemma 13:

$$\lim_{x\to 0}\frac{\sin(x)}{x} = 1. \tag{81}$$

Proof: We prove Lemma 13 by applying L'Hôpital's rule to (81) as shown next

$$\lim_{x\to 0}\frac{\frac{\partial\sin(x)}{\partial x}}{\frac{\partial x}{\partial x}} = \lim_{x\to 0}\cos(x) = 1. \tag{82}$$

□

Lemma 14:

$$\lim_{x\to\infty}\left(x\sin\left(\frac{a}{x}\right)\right)^n = a^n, \forall a, n\in\mathbb{R}. \tag{83}$$

Proof: We start by re-writing (83) as

$$\left(\lim_{x\to\infty}\frac{a}{a}\frac{\sin\left(\frac{a}{x}\right)}{\frac{1}{x}}\right)^n = \left(\lim_{x\to\infty}a\frac{\sin\left(\frac{a}{x}\right)}{\frac{a}{x}}\right)^n, \tag{84}$$

where we also used the power rule of limits to re-write it. Next, we apply the following change of variables $\theta = \frac{a}{x}$

to (84), resulting in

$$\left(\lim_{\theta\to 0} a\frac{\sin(\theta)}{\theta}\right)^n = a^n\left(\lim_{\theta\to 0}\frac{\sin(\theta)}{\theta}\right)^n, \tag{85}$$

where we used the constant multiple rule of limits to find the last part. Next, by using Lemma 13, we conclude the proof. □

A. DERIVATION OF REMARK 1

The results (14) and (15) are found after expanding (9) and (10), using Lemma 14 and the fact that $\lim_{x\to\infty}\cos(1/x) = 1$.

APPENDIX C

For the proof of (18) we should notice that when $\lim_{\rho\to\infty}\theta = \infty$ then, consequently, $\lim_{\rho\to\infty} -\frac{1}{4\theta^2} = 0$. Therefore,

$$\lim_{\rho\to\infty} {}_2F_3\left(1, 1; 2, \frac{3}{2}-\frac{\kappa}{2}, 2-\frac{\kappa}{2}; -\frac{1}{4\theta^2}\right) = 1. \tag{86}$$

$$\lim_{\rho\to\infty} {}_1F_2\left(\frac{\kappa}{2}+\frac{1}{2}; \frac{3}{2}, \frac{\kappa}{2}+\frac{3}{2}; -\frac{1}{4\theta^2}\right) = 1. \tag{87}$$

$$\lim_{\rho\to\infty} {}_1F_2\left(\frac{\kappa}{2}; \frac{1}{2}, \frac{\kappa}{2}+1; -\frac{1}{4\theta^2}\right) = 1. \tag{88}$$

Hence, in high SNR regime (17) can be tightly approximated as (18), which concludes the proof.

APPENDIX D

The proof of (19) is straightforwardly found by noticing that the first three terms of (18) tend to 0 when $\rho\to\infty$, since $\theta\to\infty$ when $\rho\to\infty$, which concludes this proof.

APPENDIX E

In high SNR regime, as $N\to\infty$ and $\kappa\to\infty$, $\Gamma(\kappa)$ grows even faster. Therefore,

$$\lim_{N\to\infty}\frac{2\pi\sec\left(\frac{\pi\kappa}{2}\right)}{(\kappa+1)\theta^{\kappa+1}\Gamma(\kappa)\log(4)} = 0. \tag{89}$$

$$\lim_{N\to\infty}\frac{2\pi\csc\left(\frac{\pi\kappa}{2}\right)}{\kappa\theta^{\kappa}\Gamma(\kappa)\log(4)} = 0. \tag{90}$$

$$\begin{aligned}
&4\sum_{l=1}^{N}\sum_{m=1}^{N}\sum_{n=m+1}^{N}\mathbb{E}\left[d_l^2 d_m d_n\cos(\delta_m-\delta_n)\right]\\
&=4\sum_{m=1}^{N}\sum_{n=1,n\neq m}^{N}\mathbb{E}\left[d_m^3 d_n\cos(\delta_m-\delta_n)\right]\\
&\quad+4\sum_{l=1}^{N}\sum_{m=1,m\neq l}^{N}\sum_{n=m+1,n\neq l}^{N}\mathbb{E}\left[d_l^2 d_m d_n\cos(\delta_m-\delta_n)\right]\\
&=4N(N-1)\mathbb{E}\left[|g_m|^3\right]\mathbb{E}\left[|h_m|^3\right]\mathbb{E}\left[|g_m|\right]\mathbb{E}\left[|h_m|\right]\mathbb{E}\left[\cos(\delta_l-\delta_m)\right]\\
&\quad+2N(N-1)(N-2)\mathbb{E}\left[|g_l|^2\right]\mathbb{E}\left[|h_l|^2\right]\mathbb{E}\left[|g_m|\right]\mathbb{E}\left[|h_m|\right]\mathbb{E}\left[|g_n|\right]\mathbb{E}\left[|h_n|\right]\cos(\delta_m-\delta_n)\\
&=\frac{1}{16}N(N-1)(2N+5)\left(\beta_g\beta_h\right)^2 Q^2\sin^2\left(\frac{\pi}{Q}\right).
\end{aligned} \tag{79}$$

$$\begin{aligned}
&4\mathbb{E}\left[\left(\sum_{m=1}^{N}\sum_{n=m+1}^{N}d_m d_n\cos(\delta_m-\delta_n)\right)^2\right]\\
&=4\sum_{j=1}^{N}\sum_{l=j+1}^{N}\sum_{m=1}^{N}\sum_{n=m+1}^{N}\mathbb{E}\left[d_j d_l d_m d_n\cos(\delta_j-\delta_l)\cos(\delta_m-\delta_n)\right]\\
&=4\sum_{j=1}^{N}\sum_{l=j+1}^{N}\sum_{m=1,m=j}^{N}\sum_{n=m+1,n=l}^{N}\mathbb{E}\left[d_j^2 d_l^2\cos^2(\delta_j-\delta_l)\right]\\
&\quad+8\sum_{l=1}^{N}\sum_{m=1,m\neq l}^{N}\sum_{n=m+1,n\neq l}^{N}\mathbb{E}\left[d_l^2 d_m d_n\cos(\delta_l-\delta_m)\cos(\delta_l-\delta_n)\right]\\
&\quad+4\sum_{j=1}^{N}\sum_{l=1,l\neq j\neq m\neq n}^{N}\sum_{m=1,l\neq j\neq m\neq n}^{N}\sum_{n=1,l\neq j\neq m\neq n}^{N}\mathbb{E}\left[d_j d_l d_m d_n\cos(\delta_j-\delta_l)\cos(\delta_m-\delta_n)\right]\\
&=\frac{N(N-1)\left(\beta_g\beta_h\right)^2\left\{Q^2\left[\pi(N-2)\sin^2\left(\frac{\pi}{Q}\right)\left(\pi\left((N-3)Q^2\sin^2\left(\frac{\pi}{Q}\right)+32\right)+16Q\sin\left(\frac{2\pi}{Q}\right)\right)-32\cos\left(\frac{4\pi}{Q}\right)\right]+32\left(Q^2+8\pi^2\right)\right\}}{256\pi^2}.
\end{aligned} \tag{80}$$

These two terms tend to 0 faster than the other two terms, concluding the proof.

APPENDIX F

Here we outline the derivation of C_{lower} in (27). We start by applying the Taylor series expansion of $1/\gamma$ around $\mathbb{E}[\gamma]$ [52], the term $\mathbb{E}[1/\gamma]$ in (26) can be approximated as [62]

$$\mathbb{E}\left[\frac{1}{\gamma}\right] \approx \frac{1}{\mathbb{E}[\gamma]} + \frac{\text{var}(\gamma)}{\mathbb{E}[\gamma]^3} = \frac{\mathbb{E}\left[\gamma^2\right]}{\mathbb{E}[\gamma]^3}. \tag{91}$$

After replacing $\mathbb{E}[\gamma]$ and $\mathbb{E}\left[\gamma^2\right]$ in (91) via (9) and (10), respectively, and then by substituting the resultant expression into (26), C_{lower} can be approximated as shown in the second part of (27).

APPENDIX G

Here we describe the derivation of the outage probability given by (36). Using the PDF of the instantaneous capacity given by (22), the outage probability can be written as

$$\begin{aligned} P_{\text{out.}} &= \Pr\{C_{\text{inst.}} < C_{\text{out.}}\} \\ &= \frac{\log(2)}{\Gamma(\kappa)\theta^{\kappa}} \int_0^{C_{\text{out.}}} 2^{u-1}(2^u-1)^{\left(\frac{\kappa-2}{2}\right)} e^{-\frac{\sqrt{2^u-1}}{\theta}} du. \end{aligned} \tag{92}$$

Next, using the following change of variable $x = 2^u - 1$, then (92) becomes

$$P_{\text{out.}} = \frac{1}{2\Gamma(\kappa)\theta^{\kappa}} \int_0^{2^{C_{\text{out.}}}-1} x^{\left(\frac{\kappa-2}{2}\right)} e^{-\frac{\sqrt{x}}{\theta}} dx. \tag{93}$$

Finally, using (2.33.10) from [52]

$$\int x^m e^{-\beta x^n} dx = -\frac{\Gamma\left(\frac{m+1}{n}, \beta x^n\right)}{n\beta^{\frac{m+1}{n}}}, \tag{94}$$

we find a solution for the integral in (93), which concludes the proof.

APPENDIX H

For the proofs of (38) and (39), we first to define the following Lemmas.

Lemma 15: According to (Eq. 8.2.5, [54])

$$1 - \frac{\Gamma(a,b)}{\Gamma(a)} = \frac{\gamma(a,b)}{\Gamma(a)}, \tag{95}$$

where $\gamma(a,b)$ is the lower incomplete gamma function.

Lemma 16: According to (Eq. 8.5.1, [54])

$$\gamma(a,b) = a^{-1}b^a\, {}_1F_1(a, a+1, -b). \tag{96}$$

Lemma 17: According to (07.20.03.0001.01) of [63]

$${}_1F_1(a,b,0) = 1. \tag{97}$$

Therefore, applying Lemmas 15 and 16, defined above, to (37) we end up with (38), which concludes the proof. Now, (39) is found by applying Lemma 17 to (38) and remembering that $\lim_{\rho\to\infty}\theta = \infty$, then $\lim_{\rho\to\infty} 1/\theta = 0$.

APPENDIX I

In this Appendix, we derive the average symbol error rate expression given by (41), but first, we need to establish some Lemmas.

Lemma 18:

$$\mathcal{Q}(x) = \frac{1}{2}\left[1 - erf\left(\frac{x}{\sqrt{2}}\right)\right]. \tag{98}$$

This relation is given by (Eq. B.111, [64]).

Lemma 19:

$$\int_0^{\infty} x^m e^{-\beta x^n} dx = \frac{\Gamma\left(\frac{m+1}{n}\right)}{n\beta^{\frac{m+1}{n}}}. \tag{99}$$

This relation is given by (Eq. 3.326.2, [52]).

Lemma 20: If erf(.) is the Gauss error function, and a, b, and $c > 0$, then the integral $\int_0^{\infty} erf(ax)\, x^b e^{-cx} dx$ is given by (100). *The integral in* (100) *is found by using an integral solver [65].*

$$\begin{aligned} \int_0^{\infty} erf(ax)\, x^b e^{-cx} dx &= c^{-b-1}\Gamma(b+1) \\ &+ \frac{ca^{-b-2}\Gamma\left(\frac{b+3}{2}\right)\, {}_2F_2\left(\frac{b}{2}+1, \frac{b}{2}+\frac{3}{2}; \frac{3}{2}, \frac{b}{2}+2; \frac{c^2}{4a^2}\right)}{\sqrt{\pi}(b+2)} \\ &- \frac{a^{-b-1}\Gamma\left(\frac{b}{2}+1\right)\, {}_2F_2\left(\frac{b}{2}+\frac{1}{2}, \frac{b}{2}+1; \frac{1}{2}, \frac{b}{2}+\frac{3}{2}; \frac{c^2}{4a^2}\right)}{\sqrt{\pi}(b+1)}. \end{aligned} \tag{100}$$

A. PROOF OF THE AVERAGE SYMBOL ERROR RATE

By using the fact that $\gamma = r^2$ (see (6)), the expectation of the conditional symbol error probability given the distribution of the SNR can be written as

$$\begin{aligned} P_e &= \mathbb{E}\left[a\mathcal{Q}\left(\sqrt{b\gamma}\right)\right] = \mathbb{E}\left[a\mathcal{Q}\left(\sqrt{br}\right)\right] \\ &= \int_0^{\infty} P_{e|\gamma}(x) f_R(x) dx, \end{aligned} \tag{101}$$

where $f_R(r)$ is the PDF of the Gamma distribution, which tightly approximates the exact PDF of the random variable, r.

By plugging $P_{e|\gamma} = a\mathcal{Q}\left(\sqrt{b\gamma}\right)$ and the Gamma PDF back into (101), the average SER is rewritten as

$$P_e = \frac{a}{\Gamma(\kappa)\theta^{\kappa}} \int_0^{\infty} \mathcal{Q}\left(\sqrt{bx}\right) x^{\kappa-1} e^{-x/\theta} dx. \tag{102}$$

By using Lemma 18, (102) can be equivalently rewritten as

$$\begin{aligned} P_e = \frac{a}{\Gamma(\kappa)\theta^{\kappa}} \Bigg[&\int_0^{\infty} x^{\kappa-1} e^{-x/\theta} dx \\ &- \int_0^{\infty} \text{erf}\left(\sqrt{\frac{b}{2}x}\right) x^{\kappa-1} e^{-x/\theta} dx \Bigg]. \end{aligned} \tag{103}$$

The first integral inside the square brackets of (103) is found by applying Lemma 19 to it, which results in

$$\int_0^{\infty} x^{\kappa-1} e^{-x/\theta} dx = \Gamma(\kappa)\theta^{\kappa}. \tag{104}$$

The second integral inside the square brackets of (103) is found by applying Lemma 20 to it, which results in

$$\int_0^\infty \operatorname{erf}\left(\sqrt{\frac{b}{2}}x\right) x^{\kappa-1} e^{-x/\theta} dx = \theta^\kappa \Gamma(\kappa) - \frac{2^{\kappa/2} b^{-\frac{\kappa}{2}} \Gamma\left(\frac{\kappa+1}{2}\right) {}_2F_2\left(\frac{\kappa}{2}+\frac{1}{2}, \frac{\kappa}{2}; \frac{1}{2}, \frac{\kappa}{2}+1; \frac{1}{2b\theta^2}\right)}{\sqrt{\pi}\kappa} + \frac{2^{\frac{\kappa+1}{2}} b^{-\frac{\kappa}{2}-\frac{1}{2}} \Gamma\left(\frac{\kappa}{2}+1\right) {}_2F_2\left(\frac{\kappa}{2}+\frac{1}{2}, \frac{\kappa}{2}+1; \frac{3}{2}, \frac{\kappa}{2}+\frac{3}{2}; \frac{1}{2b\theta^2}\right)}{\sqrt{\pi}\theta(\kappa+1)}. \quad (105)$$

Finally, by substituting (104) and (105) back into (103), we conclude the proof.

APPENDIX J

For the proof of (42) we should notice that when $\lim_{\rho\to\infty} \theta = \infty$ then, consequently, $\lim_{\rho\to\infty} \frac{1}{2\theta^2} = 0$. Therefore,

$$\lim_{\rho\to\infty} {}_2F_2\left(\frac{\kappa}{2}+\frac{1}{2}, \frac{\kappa}{2}; \frac{1}{2}, \frac{\kappa}{2}+1; \frac{1}{2b\theta^2}\right) = 1. \quad (106)$$

$$\lim_{\rho\to\infty} {}_2F_2\left(\frac{\kappa}{2}+\frac{1}{2}, \frac{\kappa}{2}+1; \frac{3}{2}, \frac{\kappa}{2}+\frac{3}{2}; \frac{1}{2b\theta^2}\right) = 1. \quad (107)$$

Hence, in high SNR regime (41) can be tightly approximated as (42), which concludes the proof.

APPENDIX K

In order to derive the diversity order, we first need to rewrite (9) and (10) as

$$\mathbb{E}[\gamma] = \rho\beta_g\beta_h\mathcal{A}_1, \quad (108)$$

and

$$\mathbb{E}\left[\gamma^2\right] = \left(\rho\beta_g\beta_h\right)^2 \mathcal{A}_2, \quad (109)$$

respectively, where $\mathcal{A}_1$ and $\mathcal{A}_2$ do not depend on the average SNR, ρ. By plugging these two equation back into (7) and (8), we find

$$\kappa = \frac{5\mathcal{A}_1^2 + \sqrt{49\mathcal{A}_1^4 - 34\mathcal{A}_1^2\mathcal{A}_2 + \mathcal{A}_2^2} - \mathcal{A}_2}{2\left(\mathcal{A}_2 - \mathcal{A}_1^2\right)} > 0, \quad (110)$$

which also does not depend on the average SNR, and

$$\theta = \rho^{\frac{1}{2}} \sqrt{\frac{\beta_g\beta_h\left(2\mathcal{A}_1^2 - \sqrt{\mathcal{A}_1^4 + 14\mathcal{A}_1^2\mathcal{A}_2 + \mathcal{A}_2^2} + 2\mathcal{A}_2\right)}{6\mathcal{A}_1}} = \rho^{\frac{1}{2}}\theta' > 0, \quad (111)$$

which depends on the average SNR. Therefore, in high-SNR regime, (42) can be written as

$$P_e^{\text{high-SNR}} \approx \mathcal{B}_1\rho^{-\frac{\kappa}{2}} - \mathcal{B}_2\rho^{-\frac{(\kappa+1)}{2}}, \quad (112)$$

where

$$\mathcal{B}_1 = \frac{a2^{-\frac{(\kappa+2)}{2}} b^{-\frac{\kappa}{2}} \theta'^{-\kappa}}{\Gamma\left(\frac{\kappa}{2}+1\right)}, \quad (113)$$

and

$$\mathcal{B}_2 = \frac{\kappa a 2^{-\frac{(\kappa+3)}{2}} b^{-\frac{(\kappa+1)}{2}} \theta'^{-(\kappa+1)}}{\Gamma\left(\frac{\kappa+3}{2}\right)}. \quad (114)$$

Note that $\mathcal{B}_1$ and $\mathcal{B}_2$ do not depend on the average SNR, *i.e.*, they are independent from it. Furthermore, from (112), we realise that the terms $\rho^{-\frac{\kappa}{2}}$ and $\rho^{-\frac{(\kappa+1)}{2}}$ contribute with diversity order of $\frac{\kappa}{2}$ and $\frac{(\kappa+1)}{2}$, respectively. Therefore, the diversity order is calculated as

$$D = \min\left(\frac{\kappa}{2}, \frac{(\kappa+1)}{2}\right). \quad (115)$$

Since $\kappa > 0$, then (115) is simplified as

$$D = \frac{\kappa}{2}. \quad (116)$$

The proof is concluded after plugging (110) into (116).

ACKNOWLEDGMENT

(Felipe A. P. de Figueiredo and Michelle S. P. Facina contributed equally to this work.)

REFERENCES

[1] W. Hou, T. Fujino, and T. Kojima, "Quantization error reduction for MIMO detection based on orthogonal lattices," *IEICE Commun. Exp.*, vol. 2, no. 2, pp. 42–48, 2013.
[2] K. Kotera, O. Muta, and H. Furukawa, "Efficient nonlinear equalization scheme for MIMO constant envelope modulation receivers affected by quantization error," in *Proc. Int. Conf. Inf. Netw.*, Feb. 2012, pp. 275–279.
[3] W. Saad, M. Bennis, and M. Chen, "A vision of 6G wireless systems: Applications, trends, technologies, and open research problems," *IEEE Netw.*, vol. 34, no. 3, pp. 134–142, May 2020.
[4] O. Ozdogan, E. Bjornson, and E. G. Larsson, "Intelligent reflecting surfaces: Physics, propagation, and pathloss modeling," *IEEE Wireless Commun. Lett.*, vol. 9, no. 5, pp. 581–585, May 2020.
[5] F. Fang, Y. Xu, Q.-V. Pham, and Z. Ding, "Energy-efficient design of IRS-NOMA networks," *IEEE Trans. Veh. Technol.*, vol. 69, no. 11, pp. 14088–14092, Nov. 2020.
[6] Q. Wu and R. Zhang, "Intelligent reflecting surface enhanced wireless network via joint active and passive beamforming," *IEEE Trans. Wireless Commun.*, vol. 18, no. 11, pp. 5394–5409, Nov. 2019.
[7] L. Dai, B. Wang, M. Wang, X. Yang, J. Tan, S. Bi, S. Xu, F. Yang, Z. Chen, M. D. Renzo, C.-B. Chae, and L. Hanzo, "Reconfigurable intelligent surface-based wireless communications: Antenna design, prototyping, and experimental results," *IEEE Access*, vol. 8, pp. 45913–45923, 2020.
[8] N. Kaina, M. Dupré, G. Lerosey, and M. Fink, "Shaping complex microwave fields in reverberating media with binary tunable metasurfaces," *Sci. Rep.*, vol. 4, no. 1, pp. 1–8, Dec. 2014.
[9] M. Dunna, C. Zhang, D. Sievenpiper, and D. Bharadia, "ScatterMIMO: Enabling virtual MIMO with smart surfaces," in *Proc. 26th Annu. Int. Conf. Mobile Comput. Netw.*, Apr. 2020, pp. 1–14.
[10] W. Tang, J. Y. Dai, M. Chen, X. Li, Q. Cheng, S. Jin, K. Wong, and T. J. Cui, "Programmable metasurface-based RF chain-free 8PSK wireless transmitter," *Electron. Lett.*, vol. 55, no. 7, pp. 417–420, Apr. 2019.
[11] W. Tang, M. Z. Chen, J. Y. Dai, Y. Zeng, X. Zhao, S. Jin, Q. Cheng, and T. J. Cui, "Wireless communications with programmable metasurface: New paradigms, opportunities, and challenges on transceiver design," *IEEE Wireless Commun.*, vol. 27, no. 2, pp. 180–187, Apr. 2020.
[12] W. Tang, J. Y. Dai, M. Z. Chen, K.-K. Wong, X. Li, X. Zhao, S. Jin, Q. Cheng, and T. J. Cui, "MIMO transmission through reconfigurable intelligent surface: System design, analysis, and implementation," *IEEE J. Sel. Areas Commun.*, vol. 38, no. 11, pp. 2683–2699, Nov. 2020.
[13] H. Zhao, Y. Shuang, M. Wei, T. J. Cui, P. D. Hougne, and L. Li, "Metasurface-assisted massive backscatter wireless communication with commodity Wi-Fi signals," *Nature Commun.*, vol. 11, no. 1, pp. 1–10, Dec. 2020.

[14] I. Yildirim, A. Uyrus, and E. Basar, "Modeling and analysis of reconfigurable intelligent surfaces for indoor and outdoor applications in future wireless networks," *IEEE Trans. Commun.*, early access, Nov. 3, 2020, doi: 10.1109/TCOMM.2020.3035391.
[15] E. Basar, M. D. Renzo, J. D. Rosny, M. Debbah, M.-S. Alouini, and R. Zhang, "Wireless communications through reconfigurable intelligent surfaces," *IEEE Access*, vol. 7, pp. 116753–116773, 2019.
[16] C. Huang, G. C. Alexandropoulos, C. Yuen, and M. Debbah, "Indoor signal focusing with deep learning designed reconfigurable intelligent surfaces," in *Proc. IEEE 20th Int. Workshop Signal Process. Adv. Wireless Commun. (SPAWC)*, Jul. 2019, pp. 1–5.
[17] J. Zhang, Z. Zheng, Z. Fei, and X. Bao, "Positioning with dual reconfigurable intelligent surfaces in millimeter-wave MIMO systems," in *Proc. IEEE/CIC Int. Conf. Commun. China (ICCC)*, Aug. 2020, pp. 800–805.
[18] K. Ntontin, A.-A. A. Boulogeorgos, D. Selimis, F. Lazarakis, A. Alexiou, and S. Chatzinotas, "Reconfigurable intelligent surface optimal placement in millimeter-wave networks," 2020, *arXiv:2011.09949*. [Online]. Available: http://arxiv.org/abs/2011.09949
[19] E. Bjornson. *Real-Time Reconfigurable Metasurfaces*. Accessed: Dec. 23, 2020. [Online]. Available: http://ma-mimo.ellintech.se/2020/12/22/real-time-reconfigurable-metasurfaces2
[20] F. A. P. D. Figueiredo. *Which Frequency Band is the Most Suitable for Ris Deployment?* Accessed: Dec. 23, 2020. [Online]. Available: https://www.researchgate.net/post/Which_frequency_band_is_the_most_suitable_for_RIS_deployment
[21] P. Wang, J. Fang, X. Yuan, Z. Chen, and H. Li, "Intelligent reflecting surface-assisted millimeter wave communications: Joint active and passive precoding design," *IEEE Trans. Veh. Technol.*, early access, Oct. 16, 2020, doi: 10.1109/TVT.2020.3031657.
[22] K. Ying, Z. Gao, S. Lyu, Y. Wu, H. Wang, and M.-S. Alouini, "GMD-based hybrid beamforming for large reconfigurable intelligent surface assisted millimeter-wave massive MIMO," *IEEE Access*, vol. 8, pp. 19530–19539, 2020.
[23] J. He, H. Wymeersch, L. Kong, O. Silven, and M. Juntti, "Large intelligent surface for positioning in millimeter wave MIMO systems," in *Proc. IEEE 91st Veh. Technol. Conf. (VTC-Spring)*, May 2020, pp. 1–5.
[24] A. M. Elbir, A. Papazafeiropoulos, P. Kourtessis, and S. Chatzinotas, "Deep channel learning for large intelligent surfaces aided mm-wave massive MIMO systems," *IEEE Wireless Commun. Lett.*, vol. 9, no. 9, pp. 1447–1451, Sep. 2020.
[25] N. S. Perovic, M. D. Renzo, and M. F. Flanagan, "Channel capacity optimization using reconfigurable intelligent surfaces in indoor mmWave environments," in *Proc. ICC-IEEE Int. Conf. Commun. (ICC)*, Jun. 2020, pp. 1–7.
[26] J. Zhang, E. Bjornson, M. Matthaiou, D. W. K. Ng, H. Yang, and D. J. Love, "Prospective multiple antenna technologies for beyond 5G," *IEEE J. Sel. Areas Commun.*, vol. 38, no. 8, pp. 1637–1660, Aug. 2020.
[27] H. Han, J. Zhao, D. Niyato, M. D. Renzo, and Q.-V. Pham, "Intelligent reflecting surface aided network: Power control for physical-layer broadcasting," in *Proc. ICC-IEEE Int. Conf. Commun. (ICC)*, Jun. 2020, pp. 1–7.
[28] R. C. Ferreira, M. S. P. Facina, F. A. P. D. Figueiredo, G. Fraidenraich, and E. R. D. Lima, "Bit error probability for large intelligent surfaces under double-nakagami fading channels," *IEEE Open J. Commun. Soc.*, vol. 1, pp. 750–759, 2020.
[29] M.-A. Badiu and J. P. Coon, "Communication through a large reflecting surface with phase errors," *IEEE Wireless Commun. Lett.*, vol. 9, no. 2, pp. 184–188, Feb. 2020.
[30] S. Abeywickrama, R. Zhang, and C. Yuen, "Intelligent reflecting surface: Practical phase shift model and beamforming optimization," in *Proc. ICC-IEEE Int. Conf. Commun. (ICC)*, Jun. 2020, pp. 1–6.
[31] Y. Han, W. Tang, S. Jin, C.-K. Wen, and X. Ma, "Large intelligent surface-assisted wireless communication exploiting statistical CSI," *IEEE Trans. Veh. Technol.*, vol. 68, no. 8, pp. 8238–8242, Aug. 2019.
[32] S. Hu, Z. Wei, Y. Cai, D. W. K. Ng, and J. Yuan, "Sum-rate maximization for multiuser MISO downlink systems with self-sustainable IRS," 2020, *arXiv:2005.11663*. [Online]. Available: https://arxiv.org/abs/2005.11663
[33] T. Wang, G. Chen, J. P. Coon, and M.-A. Badiu, "Study of intelligent reflective surface assisted communications with one-bit phase adjustments," 2020, *arXiv:2008.09770*. [Online]. Available: https://arxiv.org/abs/2008.09770
[34] D. Gesbert, H. Bolcskei, D. A. Gore, and A. J. Paulraj, "Outdoor MIMO wireless channels: Models and performance prediction," *IEEE Trans. Commun.*, vol. 50, no. 12, pp. 1926–1934, Dec. 2002.
[35] Y. Ai, M. Cheffena, A. Mathur, and H. Lei, "On physical layer security of double Rayleigh fading channels for vehicular communications," *IEEE Wireless Commun. Lett.*, vol. 7, no. 6, pp. 1038–1041, Dec. 2018.
[36] J. Salo, H. M. El-Sallabi, and P. Vainikainen, "Impact of double-Rayleigh fading on system performance," in *Proc. 1st Int. Symp. Wireless Pervasive Comput.*, Jan. 2006, p. 5.
[37] H. Shin and M. Z. Win, "MIMO diversity in the presence of double scattering," *IEEE Trans. Inf. Theory*, vol. 54, no. 7, pp. 2976–2996, Jul. 2008.
[38] M. Jung, W. Saad, Y. Jang, G. Kong, and S. Choi, "Performance analysis of large intelligent surfaces (LISs): Asymptotic data rate and channel hardening effects," *IEEE Trans. Wireless Commun.*, vol. 19, no. 3, pp. 2052–2065, Mar. 2020.
[39] H. Zhang, B. Di, L. Song, and Z. Han, "Reconfigurable intelligent surfaces assisted communications with limited phase shifts: How many phase shifts are enough?" *IEEE Trans. Veh. Technol.*, vol. 69, no. 4, pp. 4498–4502, Apr. 2020.
[40] B. Di, H. Zhang, L. Song, Y. Li, Z. Han, and H. V. Poor, "Hybrid beamforming for reconfigurable intelligent surface based multi-user communications: Achievable rates with limited discrete phase shifts," *IEEE J. Sel. Areas Commun.*, vol. 38, no. 8, pp. 1809–1822, Aug. 2020.
[41] C. Huang, G. C. Alexandropoulos, A. Zappone, M. Debbah, and C. Yuen, "Energy efficient multi-user MISO communication using low resolution large intelligent surfaces," in *Proc. IEEE Globecom Workshops (GC Wkshps)*, Dec. 2018, pp. 1–6.
[42] Y. Yang, B. Zheng, S. Zhang, and R. Zhang, "Intelligent reflecting surface meets OFDM: Protocol design and rate maximization," *IEEE Trans. Commun.*, vol. 68, no. 7, pp. 4522–4535, Jul. 2020.
[43] T. A. Tsiftsis, S. Atapattu, R. Fan, P. Dharmawansa, G. Wang, and J. Evans, "Reconfigurable intelligent surface assisted two-way communications: Performance analysis and optimization," 2020, *arXiv:2001.07907*. [Online]. Available: http://arxiv.org/abs/2001.07907
[44] T. Wang, G. Chen, J. P. Coon, and M.-A. Badiu, "Chernoff bounds and saddlepoint approximations for the outage probability in intelligent reflecting surface assisted communication systems," 2020, *arXiv:2008.05447*. [Online]. Available: http://arxiv.org/abs/2008.05447
[45] D. Kudathanthirige, D. Gunasinghe, and G. Amarasuriya, "Performance analysis of intelligent reflective surfaces for wireless communication," 2020, *arXiv:2002.05603*. [Online]. Available: http://arxiv.org/abs/2002.05603
[46] A.-A.-A. Boulogeorgos and A. Alexiou, "Performance analysis of reconfigurable intelligent surface-assisted wireless systems and comparison with relaying," *IEEE Access*, vol. 8, pp. 94463–94483, 2020.
[47] L. Yang, Y. Yang, D. B. D. Costa, and I. Trigui, "Outage probability and capacity scaling law of multiple RIS-aided cooperative networks," 2020, *arXiv:2007.13293*. [Online]. Available: http://arxiv.org/abs/2007.13293
[48] T. L. Marzetta, *Fundamentals of Massive MIMO*. Cambridge, U.K.: Cambridge Univ. Press, 2016.
[49] M. D. Renzo, F. H. Danufane, X. Xi, J. D. Rosny, and S. Tretyakov, "Analytical modeling of the path-loss for reconfigurable intelligent surfaces—Anomalous mirror or scatterer?" in *Proc. IEEE 21st Int. Workshop Signal Process. Adv. Wireless Commun. (SPAWC)*, May 2020, pp. 1–5.
[50] Q. Wu and R. Zhang, "Beamforming optimization for intelligent reflecting surface with discrete phase shifts," in *Proc. ICASSP-IEEE Int. Conf. Acoust., Speech Signal Process. (ICASSP)*, May 2019, pp. 7830–7833.
[51] E. Basar, "Transmission through large intelligent surfaces: A new frontier in wireless communications," in *Proc. Eur. Conf. Netw. Commun. (EuCNC)*, Jun. 2019, pp. 112–117.
[52] I. S. Gradshteyn and I. M. Ryzhik, *Table of Integrals, Series, and Products*, 7th ed. Amsterdam, The Netherlands: Elsevier/Academic Press, 2007.
[53] *Mathematica*, Wolfram Res., Champaign, IL, USA, 2018.
[54] F. W. J. Olver, A. B. O. Daalhuis, D. W. Lozier, B. I. Schneider, R. F. Boisvert, C. W. Clark, B. R. Miller, B. V. Saunders, H. S. Cohl, and M. A. McClain. *NIST Digital Library of Mathematical Functions, Release 1.0.25 of 2019-12-15*. Accessed: Jul. 10, 2020. [Online]. Available: http://dlmf.nist.gov/
[55] M. Abramowitz and I. A. Stegun, *Handbook of Mathematical Functions With Formulas, Graphs, and Mathematical Tables*. New York, NY, USA: Dover, 1964.
[56] J. Proakis and M. Salehi, *Digital Communications*. New York, NY, USA: McGraw-Hill, 2008.
[57] Z. Wang and G. B. Giannakis, "A simple and general parameterization quantifying performance in fading channels," *IEEE Trans. Commun.*, vol. 51, no. 8, pp. 1389–1398, Aug. 2003.
[58] F. A. P. D. Figueiredo, C. F. Dias, E. R. D. Lima, and G. Fraidenraich, "Capacity bounds for dense massive MIMO in a line-of-sight propagation environment," *Sensors*, vol. 20, no. 2, p. 520, Jan. 2020.
[59] F. A. P. D. Figueiredo, F. A. C. M. Cardoso, I. Moerman, and G. Fraidenraich, "On the application of massive MIMO systems to machine type communications," *IEEE Access*, vol. 7, pp. 2589–2611, 2019.

[60] S. Kullback and R. A. Leibler, "On information and sufficiency," *Ann. Math. Statist.*, vol. 22, no. 1, pp. 79–86, 1951.
[61] A. Papoulis and S. U. Pillai, *Probability, Random Variables, and Stochastic Processes*, 4th ed. Boston, MA, USA: McGraw-Hill, 2002.
[62] Q. Zhang, S. Jin, K.-K. Wong, H. Zhu, and M. Matthaiou, "Power scaling of uplink massive MIMO systems with arbitrary-rank channel means," *IEEE J. Sel. Topics Signal Process.*, vol. 8, no. 5, pp. 966–981, Oct. 2014.
[63] *The Wolfram Functions Site*, Wolfram Res., Champaign, IL, USA, Oct. 2001.
[64] J. Shynk, *Probability, Random Variables, and Random Processes: Theory and Signal Processing Applications*. Hoboken, NJ, USA: Wiley, 2012.
[65] *Mathematica, Version*, W. R. Inc., Champaign, IL, USA, 2020.

FELIPE A. P. DE FIGUEIREDO received the B.S. and M.S. degrees in telecommunications from the Instituto Nacional de Telecomunicações (INATEL), Minas Gerais, Brazil, in 2004 and 2011, respectively, and the Ph.D. degree from the State University of Campinas (UNICAMP), Brazil, in 2019. He has been working with the Research and Development of telecommunications systems for more than 15 years. His research interests include digital signal processing, digital communications, mobile communications, MIMO, multicarrier modulations, FPGA development, and machine learning.

MICHELLE S. P. FACINA was born in Juiz de Fora, Brazil, in 1989. She received the B.S. and M.Sc. degrees in electrical engineering from the Federal University of Juiz de Fora (UFJF), Brazil, in 2013 and 2015, respectively. She is currently pursuing the Ph.D. degree in electrical engineering with the University of Campinas (UNICAMP), Brazil. She was a Visiting Ph.D. Student with the CentraleSupelec (L2S Group), France, for one year. Her research interests include digital communication and signal processing, and applied to wireless.

RICARDO COELHO FERREIRA was born in Espirito Santo, Brazil, in 1995. He received the B.S. degree in electrical engineering from the Federal University of Ouro Preto (UFOP), Brazil, in 2018. He is currently pursuing the M.Sc. degree in electrical engineering with the University of Campinas (UNICAMP), Brazil. His research interests include digital signal processing, digital communications, random matrix theory, biological signal processing, machine learning, and electromagnetic wave propagation.

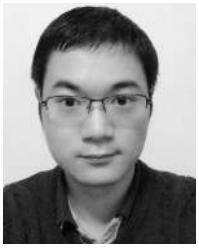

YUN AI (Member, IEEE) received the M.Sc. degree in electrical engineering from the Chalmers University of Technology, Göteborg, Sweden, in 2012, and the Ph.D. degree from the University of Oslo, Oslo, Norway, in 2018. In 2016, he was a Visiting Researcher with the Department of Information and Computer Science, Keio University, Tokyo, Japan. In 2016, he was funded by a stipend from the Norwegian University Center, Saint Petersburg, Russia. He was a Visiting Researcher with the Faculty of Applied Mathematics and Control Processes, Saint Petersburg State University, Saint Petersburg. He is currently a Researcher with the Norwegian University of Science and Technology (NTNU), Norway. He has been with the Signal Processing Group, Technische Universität Darmstadt, Darmstadt, Germany, as a Research Student, and with Ericsson as an Engineer. His current research interests include wireless communications, with a focus on communication theory, wireless sensor networks, and smart grids.

RUKHSANA RUBY received the master's degree from the University of Victoria, Canada, in 2009, and the Ph.D. degree from The University of British Columbia, Canada, in 2015. She has authored nearly 60 technical papers of well-recognized journals and conferences. Her research interest includes the management and optimization of next-generation wireless networks. She was a recipient of several awards or honors, notable among which are the Wait-listed for Canadian NSERC Postdoctoral Fellowship, the IEEE Exemplary Certificate (IEEE Communications Letters in 2018 and IEEE Wireless Communications Letters in 2018), and the Outstanding Reviewer Certificate (*Elsevier Computer Communications* in 2017). She has served as the Lead Guest Editor for the Special Issue on NOMA Techniques Under EURASIP JWCN, in 2017, and currently serving as an Associate Editor to this journal. She has also been serving as a technical program committee member in various reputed conferences.

QUOC-VIET PHAM (Member, IEEE) received the B.S. degree in electronics and telecommunications engineering from the Hanoi University of Science and Technology, Vietnam, in 2013, and the M.S. and Ph.D. degrees in telecommunications engineering from Inje University, South Korea, in 2015 and 2017, respectively. From September 2017 to December 2019, he was with Kyung Hee University, Changwon National University, and Inje University, on various academic positions. He is currently a Research Professor with the Research Institute of Computer, Information and Communication, Pusan National University, South Korea. His research interests include convex optimization, game theory, and machine learning to mobile edge/cloud computing, and resource allocation for 5G wireless networks and beyond. He received the Best Ph.D. Thesis award in Engineering from Inje University in 2017.

GUSTAVO FRAIDENRAICH was born in Pernambuco, Brazil, in 1977. He received the degree in electrical engineering from the Federal University of Pernambuco (UFPE), Brazil, and the M.Sc. and Ph.D. degrees from the State University of Campinas (UNICAMP), Brazil, in 2002 and 2006, respectively. From 2006 to 2008, he has worked as Postdoctoral Fellow with Stanford University (Star Lab Group), USA. He is currently an Assistant Professor with UNICAMP. He is also the President of the Technical Board of Venturus Company, a branch from Ericsson Company. He has published more than 50 international journal articles and more than 100 conference papers of the first line. His research interests include multiple antenna systems, cooperative systems, radar systems, and wireless communications in general. He was a recipient of the FAPESP (Fundação de Amparo à Pesquisa do Estado de São Paulo) Young Researcher Scholarship in 2009. He has been an Associate Editor of the *ETT* journal for many years.